UNIVERSITÀ DEGLI STUDI DI PARMA

DIPARTIMENTO DI FARMACIA

DOTTORATO DI RICERCA IN
BIOFARMACEUTICA-FARMACOCINETICA
XXVIII CICLO

# EFFECT OF LACTOSE SOLID-STATE ON THE AEROSOLIZATION PERFORMANCE OF DRUG-CARRIER MIXTURES

Doctorate Coordinator: Prof. RUGGERO BETTINI
Supervisor: Prof. RUGGERO BETTINI
Tutor: Dr. MICHELE MÜLLER

Ph.D. Candidate:
ANDREA DELLA BELLA

A Laura, alla mia famiglia
e ai miei amici più cari.

## Summary

## List of Symbols and Acronyms

| | |
|---|---|
| $a$ | Surface area of the probe |
| AFM | Atomic force microscopy |
| $AN^*$ | Corrected electron acceptor or acid number |
| API | Active pharmaceutical ingredient |
| BUD | Budesonide |
| $C$ | Degree of crystallinity |
| CAB | Cohesive-adhesive balance |
| COPD | Chronic obstructive pulmonary disease |
| $d_{ae}$ | Aerodynamic diameter |
| $d_{V10}$ | 10$^{th}$ percentile volume diameter |
| $d_{V50}$ | Volume median diameter |
| $d_{V90}$ | 90$^{th}$ percentile volume diameter |
| DMSO-$d_6$ | Deuterated dimethyl sulfoxide |
| $DN$ | Electron donor or base number |
| DPI | Dry powder inhaler |
| DSC | Differential scanning calorimetry |
| DVS | Dynamic vapour sorption |
| ED | Emitted dose |
| FPD | Fine particle dose |
| FPF | Fine particle fraction |
| $\gamma_L^D$ | Dispersive surface tension of the probe |
| $\gamma_S$ | Surface (free) energy |
| $\gamma_S^-$ | Base (Lewis donor) contribution of specific surface energy |
| $\gamma_S^+$ | Acid (Lewis acceptor) contribution of specific surface energy |
| $\gamma_S^D$ | Dispersive surface energy |
| $\gamma_S^{SP}$ | Specific surface energy |
| $\Delta G_A$ | Standard free energy of adsorption |
| $\Delta G_A^{SP}$ | Specific free energy of adsorption |
| GC | Gas chromatography |

| | |
|---|---|
| GSD | Geometric standard deviation |
| $^1$H NMR | Proton nuclear magnetic resonance |
| HPLC | High performance liquid chromatography |
| IGC | Inverse gas chromatography |
| IR | Infrared |
| $K_A$ | Acidic or electron accepting parameter |
| $K_D$ | Basic or electron donating parameter |
| $L_{am}$ | Amorphous lactose |
| $L\alpha{\cdot}H_2O$ | α-lactose monohydrate |
| $L\alpha_H$ | Hygroscopic anhydrous α-lactose |
| $L\alpha_S$ | Stable anhydrous α-lactose |
| Lβ | β-lactose |
| LOD | Limit of detection |
| LOQ | Limit of quantification |
| MDI | Metered-dose inhaler |
| MMAD | Mass median aerodynamic diameter |
| MOC | Micro-orifice collector |
| $N$ | Avogadro's number |
| NGI | Next generation impactor |
| NIR | Near-infrared |
| $P_{ow}$ | Octanol/water partition coefficient |
| $P_R$ | Ring pressure |
| $P_V$ | Venturi pressure |
| $R$ | Gas constant |
| $R_F$ | Feed rate |
| RH | Relative humidity |
| SEM | Scanning electron microscopy |
| SS | Salbutamol sulphate |
| $T$ | Temperature |
| $T_g$ | Glass transition temperature |
| TGA | Thermogravimetric analysis |
| UV | Ultraviolet |

| | |
|---|---|
| Vis | Visible |
| $V_N$ | Net retention volume |
| XRPD | X-ray powder diffraction |
| $y_{RH}$ | Total weight variation at RH% relative humidity |
| $y_{RH}^{am}$ | $L_{am}$ contribution to total weight variation at RH% relative humidity |
| $y_{RH}^{H}$ | $L\alpha_H$ contribution to total weight variation at RH% relative humidity |
| $y_{RH}^{S}$ | $L\alpha_S$ contribution to total weight variation at RH% relative humidity |

## List of Equations

## List of Figures

## List of Tables

# *Introduction*

# 1. INTRODUCTION

## 1.1. Inhalation Drug Delivery

The inhalation therapy is commonly used for the treatment of local respiratory diseases (Timsina et al., 1994), but it can be employed to obtain a systemic effect as well (Colombo et al., 2013). In fact, despite drug administration by inhalation has originally been focused on the treatment of diseases like asthma and COPD (chronic obstructive pulmonary disease), new areas have recently become of great interest: antibiotic therapies against infectious diseases which develop in the lungs (e.g., tuberculosis and cystic fibrosis), vaccinations against viral diseases (e.g., influenza and measles) or systematically acting drugs with poor-to-no bioavailability when administered via the traditional oral route (e.g., proteins and peptides) (Hoppentocht et al., 2014).

Compared to the oral route, inhalation shows some advantages. First of all, the lung has a huge surface area (> 100 $m^2$) available for drug adsorption, it is richly vascularized and characterized by good epithelial permeability; this ensures a predictable transport of the drug and a rapid onset of action. Moreover, the absence of the first-pass effect and the enzymatic degradation typical of the gastrointenstinal tract allows for the administration of lower doses of drug, thus reducing the risk of undesired side effects (Aulton and Taylor, 2013).

On the other hand, a fundamental and specific issue is represented by the fact that, to obtain a suitable bioavailability, the drug has to be efficiently deposited in the lower airways. This means that it should be formulated in a proper way in order to be respirable. The branched structure of the lungs represents an efficient aerodynamic filter which hinders the access and deposition of exogenous agents (such as drugs) in the lower

airways. The respiratory tract is usually described by referring to Weibel's model (Weibel, 1963), that distinguishes 23 subsequent bifurcations starting at the trachea (generation 0) and finishing at the alveolar sacs (generation 23) (Frijlink and De Boer, 2004) (Figure 1). Two main compartments can be identified: the conducting region (generations 0-16) and the respiratory region (generations 17-23). The conducting airways are represented by the trachea that bifurcates into two principal bronchi (right and left), which in turn branch in bronchioles with a progressively smaller diameter. The function of this region is to transport the air from the external environment into the lungs and vice versa. The respiratory airways start with the respiratory bronchioles and include all the structures that participate in the gas exchange (i.e., alveolar ducts and sacs).

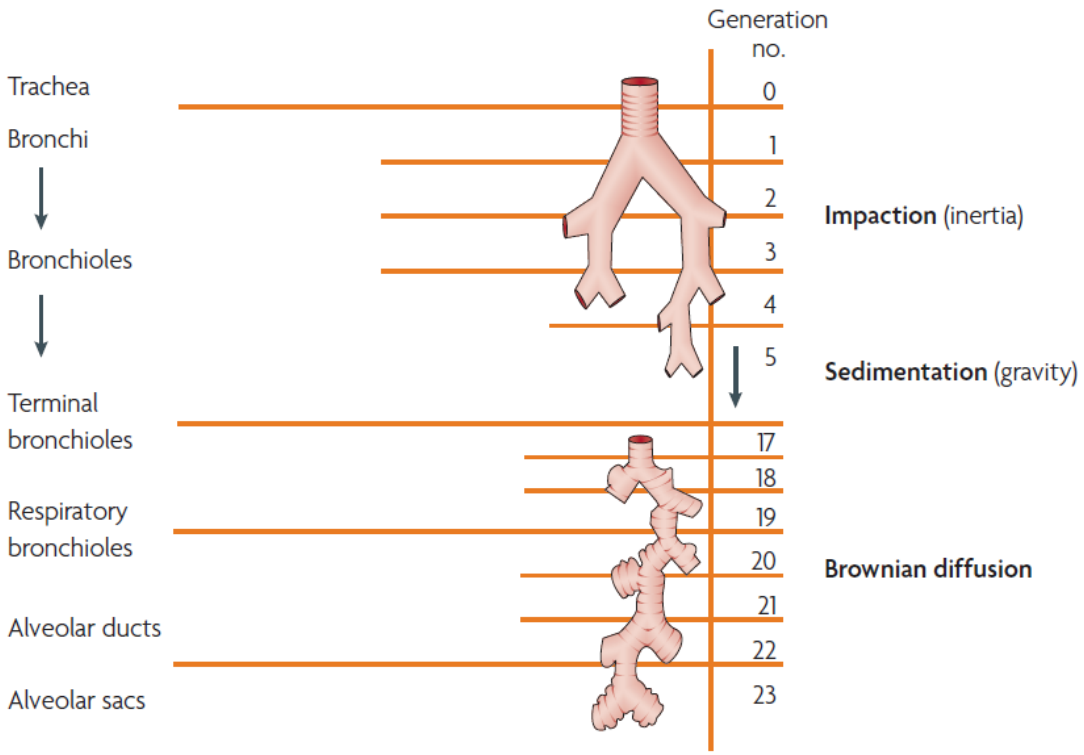


**Figure 1** Schematic representation of the lung structure and principal deposition mechanisms (Patton and Byron, 2007, reprinted with permission).

The two main factors that affect the lung function are: the progressive decrease of the

airway diameter (from 18 mm in the trachea (for adults) to 0.4 mm in the alveolar sacs), that allows the penetration of air in the deep lung, and the concomitant increase of the surface area, that promotes an efficient gas exchange between the alveolar space and the blood in the pulmonary capillaries.

Given the complexity of the above-described structure, the deposition of particles in the airways is a very complicated process. Inhaled particles can deposit or be captured in each point of the respiratory tract as a result of different mechanisms: impaction, sedimentation and diffusion (Figure 1). Impaction is particularly relevant in the upper airways and for larger particles, whose inertia makes them to leave the streamline of the airflow and collide with the walls of an airway duct (Patton and Byron, 2007). In the middle airways, slightly smaller particles deposit by sedimentation under the influence of gravity. In the alveolar region, deposition by Brownian diffusion (the irregular motion of an aerosol particle in still air caused by random variations in the incessant bombardment of gas molecules against the particle) gains importance, especially for particles in the submicron range (Frijlink and De Boer, 2004). Furthermore, deposition in the respiratory tract may occur by electrostatic precipitation or interception. The first situation is encountered when an electrically charged particle approaches a surface in the airways inducing an opposite charge on it. Particle deposition may take place as a consequence of the attractive force arising between the opposite charges. Finally, interception is particularly relevant when the dimension of the particles is comparable to the airway radius and especially in the case of fibres or needle-like particles (Aulton and Taylor, 2013).

The entity and the site of deposition inside the lung are strongly dependent on both patient's features (lung geometry, age, gender, way of breathing) and aerosol physical properties, such as particle size, density, shape, hygroscopicity and electric charge.

Among these factors, the one that mostly affects deposition in the respiratory tract is the dimension of the particles, that is represented by the aerodynamic diameter ($d_{ae}$). The aerodynamic diameter is defined as the diameter of a sphere with unit density that has the same sedimentation velocity of the particle under study and can be mathematically calculated based on the following equation:

$$d_{ae} = d_V \sqrt{\frac{\rho}{\rho_0 \chi}} \quad [1]$$

where $d_V$ is the estimated particle geometric diameter (or equivalent volume diameter), $\rho$ the density of the particle, $\rho_0$ the unit density and $\chi$ the dynamic shape factor (equal to 1 in the case of a sphere). The dynamic shape factor is the ratio of the actual resistance force experienced by the non-spherical particle falling in the air to the resistance force experienced by a sphere having the same volume (Telko and Hickey, 2005).

Hence, it is the particle aerodynamic diameter, rather than its geometric size, that mainly determines lung deposition. The majority of the particles bigger than 10 μm deposits in the upper respiratory tract (i.e., oropharynx) due to inertial impaction caused by their "considerable" mass. Particles with an aerodynamic diameter lower than 5 μm pass through the upper airways and deposit in the lower ones (i.e., bronchial tree and alveoli) under the influence of gravitational sedimentation and Brownian motion. It is a common believing that excessively small particles ($d_{ae}$ < 0.5 μm) are withdrawn by the airflow and exhaled, though some recent studies postulate different hypotheses (Kirch et al., 2012). In conclusion, to obtain a good distribution throughout the lung, particles need to be in the 1-5 μm aerodynamic diameter range.

For heterodisperse aerosols, the dimensional distribution is described by the mass median aerodynamic diameter (MMAD), which represents the particle size that divides the distribution in half as a function of mass. In addition, in the case of a log-normal distribution, the variability of the particle diameters within the aerosol is represented by the geometric standard deviation (GSD), which is usually calculated by dividing the particle size at the $84^{th}$ percentile on the cumulative distribution by the median size (Telko and Hickey, 2005).

As previously mentioned, particle deposition into the lungs may be influenced by other parameters, such as density, shape and hygroscopicity. The aerodynamic diameter of a particle is a function of the square root of its density. This means that, for a particle with a given geometric diameter, a density reduction will result in a smaller aerodynamic diameter. In this way, it is possible to use, for example, larger particles that show a good aerodynamic behaviour being at the same time more manageable. Shape might be a relevant factor as well. Elongated or needle-shaped particles have aerodynamic diameters that are essentially independent from the length and almost equal to the shortest dimension. Thus, they may exhibit the same aerodynamic diameter of a spherical particle with the same mass or volume. Hygroscopicity is the intrinsic tendency of a material to absorb moisture from the surrounding environment. Since the lung has a relative humidity (RH) of approximately 99.5%, hygroscopic aerosol particles may be subject to moisture uptake, which leads to an increase in the particle size and definitely affects lung deposition (Telko and Hickey, 2005). All these factors must be taken into account in order to provide an efficient and effective inhalation drug delivery.

Furthermore, the inhalation product is probably the most complex among the pharmaceutical dosage forms, being composed, not only by the active pharmaceutical

ingredient (API) and the formulation, but also by the inhalation device, that is strongly related to the formulation itself. There are three different kinds of inhalation devices: nebulizers, metered-dose inhalers (MDIs) and dry powder inhalers (DPIs).

## 1.2. Dry Powder Inhalers (DPIs)

Dry powder inhalers were introduced on the market since the early 1970s (Spinhaler® (Fisons)) and got progressively diffused, especially in Europe, where today they are used for the treatment of asthma and COPD by more than the 40% of the patients (Atkins, 2005; Marriott and Frijlink, 2012).

DPIs are composed of a powder formulation in an inhaler device, which generally includes some fundamental elements: a mechanism containing or metering a single drug dose, a powder de-agglomeration principle dispersing the powder in the inhaled air stream and a mouthpiece (Frijlink and De Boer, 2004).

Compared to other inhalation devices, they exhibit several advantages. The powder aerosolization is usually produced through a mechanical method that introduces energy in the powder bed and is directly activated by the inspiration of the patient (breath-operated inhalers). Thus, DPIs are handy and easy to use since they require little or no coordination between device actuation and inhalation (Figure 2). They are cheaper compared to nebulizers and, differently from MDIs, they do not contain propellants. Finally, they employ solid formulations that usually have higher physico-chemical and microbiological stability than solutions or suspensions.

**Figure 2** How to use a DPI[1].

In terms of design, DPIs can be classified as single- or multi-dose systems (Colombo et al., 2013) (Figure 3). Single-dose systems (e.g., HandiHaler® (Boehringer Ingelheim) and

[1] http://www.tobipodhaler.com/c/taking-tobi-podhaler1, visited on January 22nd, 2016.

Podhaler™ (Novartis)) generally use pre-filled capsules which are inserted into the device and pierced by the patient before inhalation. After use, the empty capsule must be discarded and replaced with a new one for the next dose. Multi-dose DPIs are usually more complex and include also a dose counting mechanism that helps the patient to understand whether the dose has been properly administered and when the device need to be replaced (Berkenfeld et al., 2015). The powder formulation may be stored in a reservoir and metered by the device (e.g., Turbuhaler® (AstraZeneca) and NEXThaler® (Chiesi)) or contained in blisters (multiple unit-dose systems, e.g., Diskhaler® and Diskus® (GlaxoSmithKline)). Compared to reservoir systems, multiple unit-dose systems usually provide a higher precision in the dosage of the drug and a better protection from the external environment.


**Figure 3** Examples of DPIs with different design: single-dose (left, Podhaler™ (Novartis)[2]), multi-dose (middle, NEXThaler® (Chiesi)[3]), multiple unit-dose (right, Diskus® (GlaxoSmithKline)[4]).

The aerosolization performance of a formulation-device combination is commonly evaluated through *in vitro* deposition tests by using the impactors recommended by the Pharmacopoeia (Ph. Eur. 8.0, 2.9.18). The aerodynamic assessment methods of fine

[2] http://www.tobipodhaler.com/c/about-tobi-podhaler, visited on January 22nd, 2016.
[3] http://www.cambridgeconsultants.com/news/pr/release/124/en, visited on January 22nd, 2016.
[4] http://www.rtmagazine.com/2015/10/advair-diskus-achieves-primary-endpoint-in-laba-safety-study/, visited on January 22nd, 2016.

particles allow to determine the fine particle dose (FPD), namely the amount of drug particles with an aerodynamic (or cut-off) diameter lower than 5 µm. From the ratio of the FPD to the emitted dose (ED, the quantity of drug exiting the device after inhalation) it is possible to obtain the fine particle fraction (FPF), that is commonly used to evaluate DPI performance.

An ideal inhaler should be cheap, easy to use and able to provide high reproducible fine fractions. Actually, DPIs are very complex systems and their performance depends on many aspects: the airflow generated by the patient, the inhaler design (with particular emphasis on the aerosolization mechanism) and the characteristics of the powder formulation (Frijlink and De Boer, 2004).

All the commercially available DPIs are "passive" systems. This means that they are activated by the patient's inspiration. The energy provided by the patient's airflow allows the fluidization of the powder bed and generates the aerosol that is eventually inhaled. Patients may have different lung capacities and produce variable flow rates depending on their age, gender and pathology. Thus, a good device should be able to produce a consistent aerosolization at reasonable flow rates and ensure flow rate independent performance. High delivery efficiency and reproducibility might be achieved by "active" inhalers, which rely on auxiliary energy (e.g., electromechanical mechanisms or pressurised air) to operate. However, none of these devices is currently available on the market.

Moreover, DPIs, and in particular single-dose devices, may be problematic for patients with dexterity issues (e.g., elderly), since their use often requires to follow multiple steps or specific cleaning routines. For this reason, an adequate training prior to product use is recommended.

As previously mentioned, another key factor in determining the performance of a DPI is the powder formulation, that should be perfectly integrated with the inhaler itself. An optimal drug delivery will be obtained only achieving a good balance between the interparticulate forces in the powder formulation, the dispersion forces generated inside the inhaler during inhalation and the deposition forces in the human respiratory tract (Hoppentocht et al., 2014) (Figure 4).

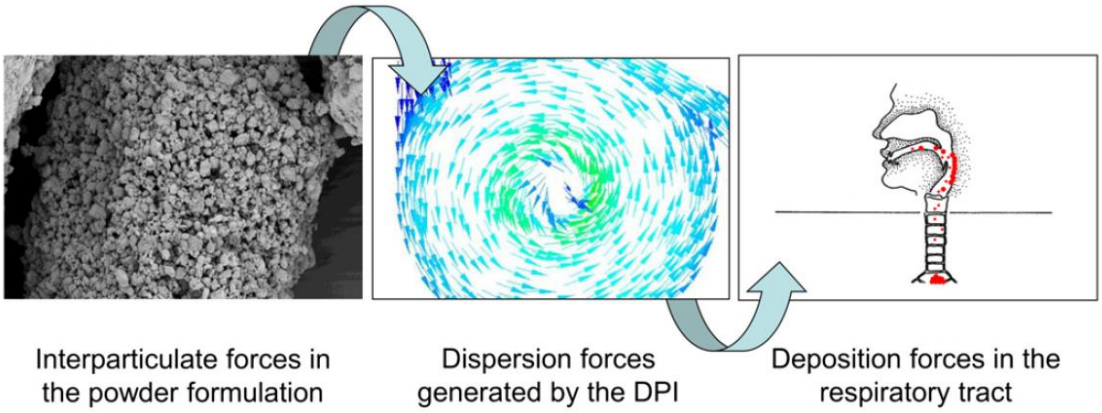


**Figure 4** Main forces determining drug delivery into the lungs (Hoppentocht et al., 2014).

Although DPIs have been widely studied in the past 40 years, a full understanding of the phenomena and mechanisms underlying their performance has not been accomplished yet. This is the reason why, despite a progressive improvement, many of the products currently commercialized show relatively poor efficiencies with fine particle fractions lower than 30% (Berkenfeld et al., 2015; Smith and Parry-Billings, 2003).

In an attempt to further improve DPI performance, in the last years, a significant amount of research activity has been focused on the development and optimization of different kinds of powder formulations.

## 1.3. Powder Formulations for Inhalation

To achieve deposition in the lower airways, drugs are commonly micronized to sizes between 1 and 5 μm (Pilcer et al., 2012). However, these fine particles are highly cohesive and have poor flow properties, thus making handling and metering particularly complicated. In order to overcome these issues and improve powder dispersibility, different strategies have been adopted, leading to the development of three types of formulations: "large" porous particles, agglomerates (also referred to as soft spherical pellets) and carrier-based formulations (or adhesive mixtures).

### 1.3.1. Porous Particles

As previously reported, the aerodynamic diameter of a particle can be reduced by decreasing its equivalent volume diameter, reducing the density or increasing the dynamic shape factor. These results can be achieved through particle engineering, that is the controlled production of particles with optimized characteristics in terms of size, morphology and structure. Particle engineering encompasses technologies such as spray drying, supercritical fluid processing, etc. and aims at the production of particles with desirable attributes, such as narrow particle size distribution, enhanced dispersibility, improved stability and optimal bioavailability (Chow et al., 2007). Porous or hollow particles, which can be produced using this approach, are particularly suitable for

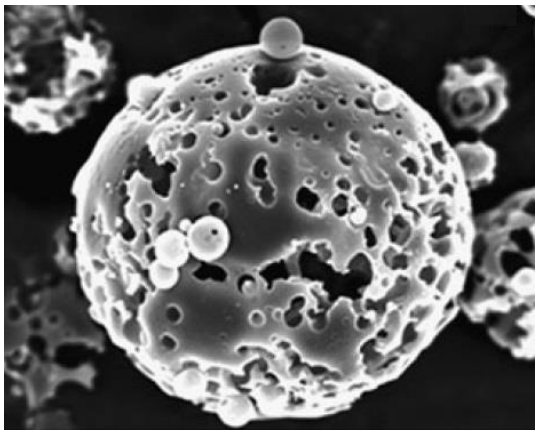

**Figure 5** Porous/hollow tobramycin particles (PulmoSphere™) (Geller et al., 2011).

pulmonary drug delivery, because they have relatively large geometric diameters and at the same time small aerodynamic diameters (Figure 5). Therefore, they exhibit a lower tendency to aggregate and can be easily dispersed. This permits, for example, the pulmonary delivery of particles with geometric particle size up to 20 µm (Edwards et al., 1997). However, a limit of this approach is represented by the fact that peripheral airways are very small and such particles may deposit by interception before reaching the deep lung. Moreover, a low density implies a reduced mass per volume, thus restricting their application to drugs with high potency and low dosage (Telko and Hickey, 2005).

### 1.3.2. Agglomerates

Another strategy to overcome the issues related to the reduced dimension of drug particles is the controlled agglomeration into soft pellets by spheronization (Claus et al., 2014). These loose agglomerates are composed by primary microparticles held together by weak interactions (Figure 6). Soft pellets are strong enough to be handled but, thanks to the turbulence generated during inhalation, they can easily break up into primary particles of respirable size (chimerical agglomerates). Since this approach does not necessarily require the use of excipients, soft pellets can be considered as a good option for the delivery of high dose drugs (mg-range). The main drawback is represented by the fact that they put great demands on the production process and on the

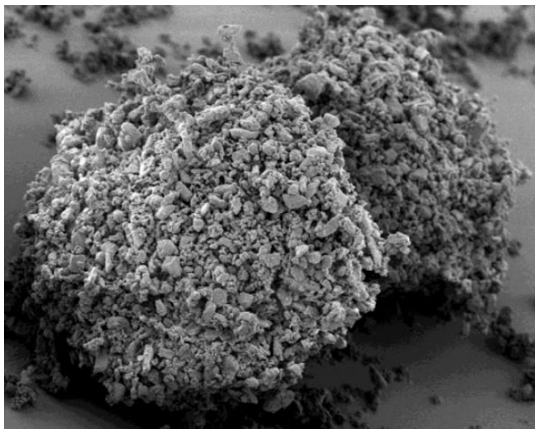

**Figure 6** Soft pellets (Hoppentocht et al., 2014).

accuracy of the dose metering system in the inhaler (Hoppentocht et al., 2014). Moreover, agglomerates are quite sensitive to humidity; moisture uptake may harden their surface and prevent a proper de-agglomeration. Among the currently marketed inhalers, only the Turbuhaler® (AstraZeneca) contains soft pellet formulations.

### 1.3.3. Carrier-Based Formulations

The most popular approach to obtain respirable powders is represented by carrier-based systems, namely formulations consisting of two components: the drug and the carrier. Micron-sized drug particles are blended with coarser (30-150 μm) carrier particles to which they adhere, thus forming the so called adhesive mixtures (de Boer et al., 2012) (Figure 7).

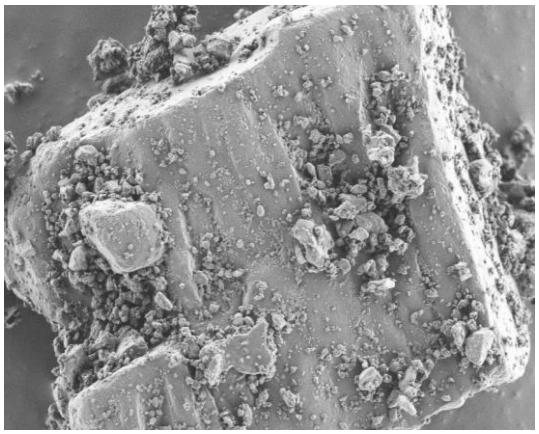

**Figure 7** Drug particles stuck on the carrier surface within an adhesive mixture.

Due to its safe toxicological profile, physico-chemical stability and compatibility with the majority of low molecular weight drugs and to the fact that it is inexpensive and readily available, lactose (in particular α-lactose monohydrate) is the most commonly used carrier (Pilcer et al., 2012).

The carrier provides bulk, facilitates handling and metering of the drug and aids in dispersion. Inside these systems the interparticulate forces have to be strong enough to produce a stable and homogeneous mixture (without segregation phenomena), but at the same time weak enough to allow the detachment of the drug from the carrier upon inhalation. Then, the delivery of the drug takes place through three different processes:

the detachment from the carrier (which remains in the inhalation device or deposits in the oropharyngeal region), the dispersion in the airflow and the deposition in the respiratory tract (Figure 8).

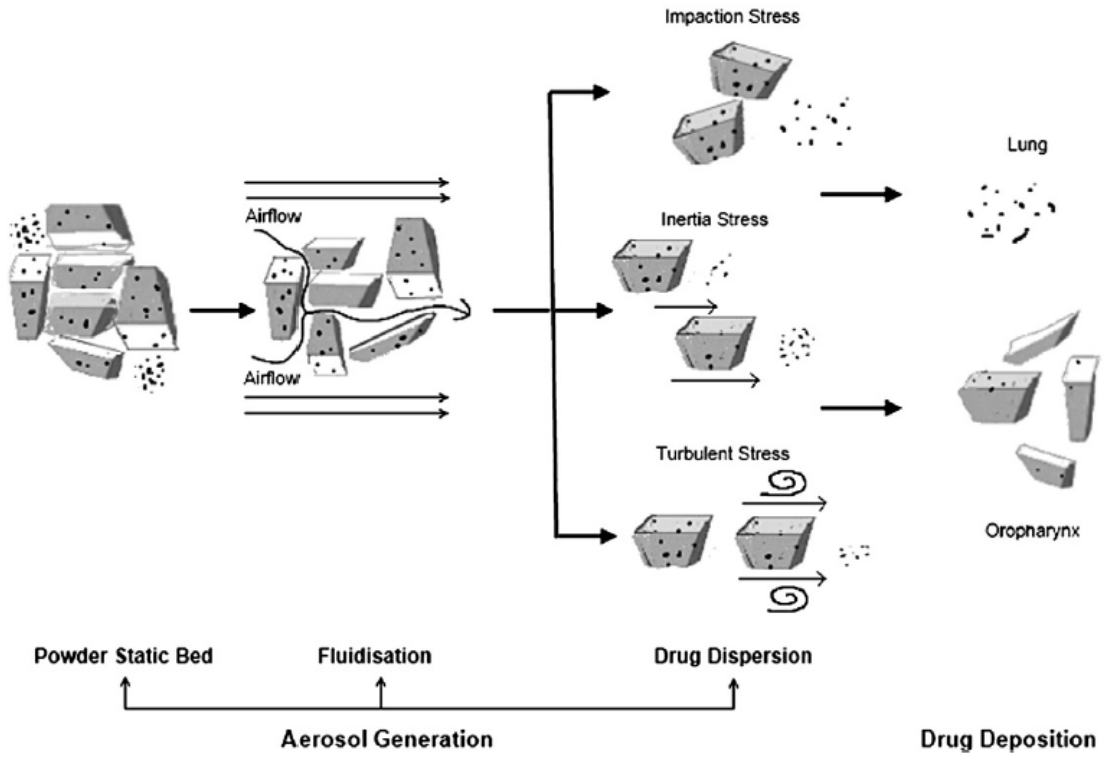


**Figure 8** Aerosol generation and drug deposition (Pilcer et al., 2012, reprinted with permission).

Due to the "limited" loading capacity of the carrier, adhesive mixtures are more suitable for low dose drugs (µg-range). Typical drug-to-carrier ratios are 1:67.5 or 1:99 (Guenette et al., 2009; Pilcer et al., 2012). Since the carrier is, by far, the most abundant component in the formulation, its physico-chemical properties are crucial in determining the performance of the product. This strongly depends on the balance between drug-carrier interparticulate forces and dispersion forces generated inside the inhaler device during inhalation. An excessively strong interaction between drug and carrier will result in the incomplete detachment of the drug with consequent poor lung deposition. Inadequate detachment of the drug from the carrier can be considered the major responsible for the

low efficiency of many DPIs (Smith and Parry-Billings, 2003). Therefore, the accurate choice of a carrier with selected characteristics is a key step in the optimization of DPI performance. As evidence of this, in the past 40 years over 250 studies have been published on the role of lactose in adhesive mixtures for inhalation (Marriott and Frijlink, 2012).

## Interparticulate Interactions

When considering adhesive mixtures, the study of the interactions between carrier and drug is of paramount importance for a good understanding of the processes that finally determine the performance of the product. One of the most problematic aspect is represented by the presence of interparticulate forces that prevent the disaggregation of the powder, thus compromising the efficiency of drug delivery into the lungs. These interparticulate interactions (both cohesion between drug-drug particles and adhesion between carrier-drug particles) are the result of physical and chemical forces: van der Waals (proximity) forces and mechanical interlocking due to the presence of defects (e.g., clefts and asperities) on the surface of the carrier, electrostatic and capillary forces, forces deriving from the presence of impurities or amorphous regions, specific (acid-base) interaction forces and hydrogen bonding (Hickey et al., 2007) (Figure 9).

In carrier-based formulations, the size difference between a micronized drug particle and a carrier particle allows to consider their interaction (adhesion) as that between a sphere and a flat surface. Van der Waals and electrical forces are proportional to the diameter of the micronized drug particle and vary with its distance from the carrier. Capillary forces are affected by the surface tension of the liquid between particles (Pilcer et al., 2012).

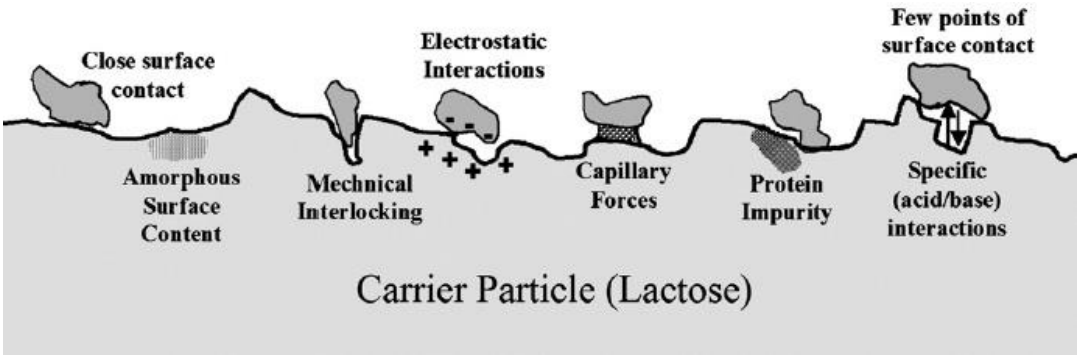


**Figure 9** Possible causes of interactions between carrier and fine (i.e., drug or excipient) particles (Pilcer et al., 2012, reprinted with permission).

Van der Waals forces are low attractive dipole-dipole forces and are the most dominant interparticulate interactions determining adhesion and cohesion within a powder formulation. Being dependent on the distance between particles, these forces are influenced by surface roughness. Highly corrugated surfaces with pronounced asperities may increase the distance between two particles and limit van der Waals interactions. On the other hand, van der Waals forces strongly increase in the case of large contact areas when, for example, protuberances fit into cavities (mechanical interlocking).

Capillary forces are attractive forces related to the formation of a concave-shaped meniscus (liquid bridge) due to the condensation of water vapour around the contact area of two contiguous surfaces. The intensity of such forces is affected by surface characteristics (e.g., roughness and physico-chemical properties) and, overall, by the environmental relative humidity.

Electrostatic interactions can be attractive or repulsive depending on whether they involve particle with opposite charge or the same charge. Electrostatic charges arise from triboelectrification, that is a type of contact electrification in which certain materials become electrically charged after being brought into contact by short collision or by intense friction. Triboelectrification mainly occurs as a consequence of manufacturing

processes such as mixing and handling, but it can appear also during the fluidization of the powder bed inside the inhaler device. Electrostatic interactions are relevant in the formation and maintenance of the adhesive mixture, the detachment of drug particles from the carrier and their deposition in the respiratory tract (electrostatic interception). Moreover, they can be strongly influenced by relative humidity. During storage, high RH conditions may lead to a reduction of electrostatic interactions, since the formation of water layers around particles enhances the surface conductivity and favours the dissipation of the charges. On the other hand, these conditions favour capillary condensation and, consequently, stronger capillary interactions.

The above-described physical interactions are barriers to the aerosol generation. In an ideal formulation, the adhesive interaction between carrier and drug particles should be overcome by the external forces (e.g., inertial, lift, drag, friction and shear forces) produced by the inspiration airflow through the inhaler. Unfortunately, due to the complexity and heterogeneity of powder systems, it is extremely difficult to consider and control each type of interaction separately.

## Carrier Properties and Their Effect on DPI Performance

The adhesion of the drug particles to the carrier is essentially a surface-interaction phenomenon. The intensity of the interaction mainly depends on the surface properties of the carrier and the drug and will be proportional to the sum of the surface energies of each component and the effective contact area between the two contiguous surfaces (Colombo et al., 2013). For this reason, the modification of the characteristics of the drug, and especially of the carrier, has become a common strategy to improve DPI performance. In

particular, carrier roughness, particle size, shape and crystal form, as well as manufacturing-induced physico-chemical changes, have proven to significantly influence the aerosol performance (Kou et al., 2012).

Several studies have been focused on the modification of the surface roughness of lactose carrier particles and its effect on the product performance. Increased surface roughness may be induced by the production process (e.g., milling) or can be achieved by recrystallization, spray drying, coating or mechanofusion (Kou et al., 2012). The roughness of the carrier particles strongly affects the area of contact with the drug particles and consequently the intensity of the adhesion forces.

In many cases, the increase of the surface smoothness of lactose particles has been reported to improve DPI performance (Iida et al., 2003; Young et al., 2002; Zeng et al., 2000b). Surface smoothing has been achieved by following different approaches. Smooth lactose particles have been produced through recrystallization from a neutralized Carbopol gel (Larhrib et al., 2003a; Zeng et al., 2001b). Ferrari et al. drastically lowered the roughness of lactose particles by means of a wet-smoothing process performed in a high-shear mixer using a water/ethanol solution. Smoothing was further improved when magnesium stearate was dispersed in the hydroalcoholic solution (Ferrari et al., 2004). Furthermore, increased smoothness was achieved by submersion of lactose particles in a water/ethanol solution for 10 minutes to partially dissolve the surface, followed by filtering and drying of the resultant particles (Dickhoff et al., 2006).

Interestingly, in this case the increased smoothness of the carrier surface led to reduced drug detachment during inhalation. This outcome was partly attributed to the removal of the adhering lactose fines, which resulted in an enhanced effectiveness of the press-on forces during mixing, with consequent increase of the adhesive forces in the mixture.

Other studies reported that rougher carrier surfaces allowed more drug particles to be emitted from the inhaler, but provided lower respirable fractions (Heng et al., 2000; Kawashima et al., 1998). Having a higher surface area, corrugated lactose particles could carry a bigger amount of drug particles, but at the same time held them more firmly due to the increased adhesion forces. The authors speculated that a microscopically increased surface roughness was desirable to improve the inhalation efficiency of DPIs (Kawashima et al., 1998).

Drug separation from the carrier during inhalation has been described as a process occurring through two major mechanisms: detachment by the flow stream (fluid forces) and detachment by impaction (mechanical forces) (Voss and Finlay, 2002). Detachment by flow is favoured by smooth carrier surfaces, since the absence of asperities allow the flow stream an unobstructed path to remove drug particles. On the other hand, detachment by impaction is mostly influenced by particle mass and is not limited by carrier roughness to the same degree as detachment by flow. Thus, it was postulated that the influence of carrier roughness on the aerosolization performance essentially consists in shifting the detachment mechanism to rely on mechanical rather than fluid forces (Donovan and Smyth, 2010). In fact, since drug particles are sheltered within cavities and asperities on the carrier surface, their detachment will be likely caused by the mechanical forces arising from the collision of the carrier particles with the inhaler walls.

All these results may appear contradictory, but it should be considered that surface force balance depends on many additional variable other than carrier roughness. Moreover, depending on the scale of the roughness, opposite effects may be produced. A highly corrugated carrier surface might “entrap” drug particles which will hardly detach during inhalation (mechanical interlocking). An excessively smooth surface may result in a large

contact area leading to strong adhesive interaction with the drug particles. Therefore, the adhesion forces will be drastically reduced only when the irregularities on the carrier surface are of such a scale that the total contact area between carrier and drug is minimized (Figure 10).

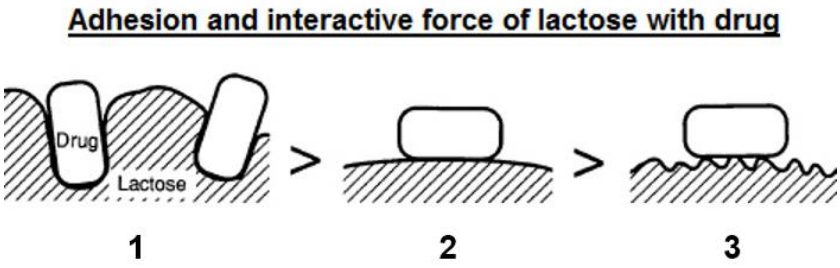


**Figure 10** Influence of carrier roughness on drug adhesion forces (micrometered topography (1), flat surface (2), nanometered topography (3)) (Kawashima et al., 1998, reprinted with permission).

The effect of carrier particle size and particle size distribution has been investigated as well (Donovan and Smyth, 2010; Zeng et al., 2000a). Different lactose size fractions were employed as carriers in the preparation of formulations for inhalation. Mixtures containing higher amounts of fine (< 10 µm) carrier particles afforded improved aerosolization performance (Guenette et al., 2009). Kaialy et al. found that the smaller was the particle size of lactose, the higher were the emitted dose and fine particle fraction. However, higher drug aerosolization efficiency was balanced by disadvantages such as poor flowability and poor dose uniformity (Kaialy et al., 2012a). In general, the presence of intrinsic lactose fines generated as a consequence of the production process (e.g., milling) positively affected the performance of DPI formulations (Steckel et al., 2006). A linear correlation between FPF and fine lactose content (up to 15%) was found (Young et al., 2007). The addition of extra fine lactose particles into a formulation is a strategy commonly used to improve DPI performance and will be further discussed below.

The carrier particle shape is another factor that can play an important role in determining the fine particle fraction of a drug (Larhrib et al., 2003a; Zeng et al., 2000a; Zeng et al., 2000b). Lactose crystals with specific morphology can be produced through controlled crystallization conditions by varying the temperature, the initial concentration of lactose, the type and/or the amount of water-miscible organic solvent used (Larhrib et al., 2003b; Zeng et al., 2000c). Increasing the elongation ratio of the lactose carrier particles generally resulted in an increase in the FPF of the drug. As previously mentioned, elongated and needle-shaped particles may exhibit a much smaller aerodynamic diameter than spherical particles of similar mass or volume. Being more aerodynamic, they may be expected to travel longer distances before impaction occurs, thus favouring deep lung penetration.

Another possibility to alter DPI performance is by employing, as carrier, different polymorphic forms of lactose. Larhrib et al. observed that commercial anhydrous lactose was able to give FPF and FPD of salbutamol sulphate significantly higher than those obtained with the conventional α-lactose monohydrate (Larhrib et al., 1999). However, the authors postulated that the more efficient drug delivery from anhydrous lactose was partly due to the higher percentage of intrinsic carrier fines present in the powder. A more recent study reported that anhydrous and monohydrate grades of lactose provided from the same supplier were not able to produce any significant difference in the FPD of budesonide (Pitchayajittipong et al., 2010). Traini et al. demonstrated the dominant role of surface chemistry in determining particle adhesion (Traini et al., 2008). The effect of four lactose pseudopolymorphs (α-lactose monohydrate, stable anhydrous α-lactose, commercial β-lactose and purified β-lactose) on the aerosolization performance of formulations containing salbutamol sulphate was investigated. The obtained results were

opposite to those previously reported by Larhrib et al. (Larhrib et al., 1999), with α-lactose monohydrate giving in this case the highest FPF. Moreover, a linear inverse relationship between carrier surface energy (measured by inverse gas chromatography) and FPF was highlighted. This is plausible considering that an increase in the surface energy usually results in an enhanced particle adhesion (with consequent poor detachment of the drug).

Inverse gas chromatography (IGC) and atomic force microscopy (AFM) are the most commonly used techniques to evaluate the interaction between carrier and drug. While IGC is capable to determine the dispersive and specific components of the surface (free) energy of a given sample (Jones et al., 2012; Tong et al., 2002), AFM colloid probe technique allows the quantification of the cohesive-adhesive balance (CAB) within a powder formulation (Begat et al., 2004a, b). Both techniques have been used in an attempt to predict DPI performance (Cline and Dalby, 2002; Jones et al., 2008a; Jones et al., 2012).

Finally, other aspects that can potentially influence DPI performance are the process-induced physico-chemical alteration (e.g., amorphization) of the carrier surface, the presence of impurities, the type of drug and its concentration and external factors such as the mixing process through which lactose-drug formulations are prepared, the environmental conditions (in particular relative humidity), the inhaler device employed and the inspiratory flow provided by the patient.

In general, it is complicated to ascribe a specific effect to each of the variables described in this paragraph and, in this sense, many different and sometimes conflicting results have been reported so far. This is partly due to the fact that all these parameters are interconnected and should be considered as a whole rather than individually (Zeng et al., 2001a). Hence, the thorough understanding of the phenomena that govern the behaviour

of inhalation powders still remains an open issue (de Boer et al., 2012; Kou et al., 2012; Pilcer et al., 2012).

## Ternary Mixtures

A strategy that has been frequently reported to have a positive effect on the aerosolization performance of adhesive mixtures is the addition of fines (fine lactose particles with a similar size to that of the drug) to the formulation, thus obtaining a ternary mixture (Zeng et al., 1998). Formulations containing an increased percentage of fines (up to a certain extent) and/or fines with a reduced size generally resulted in improved FPFs. However, the presence of larger carrier particles remained essential and excessive amounts of fines negatively affected powder flowability, mixing homogeneity and long-term stability (especially in conditions of high RH) (Guenette et al., 2009; Louey et al., 2003; Young et al., 2007).

The mechanism of action of these fines has not been completely understood so far. Two different theories have been formulated: the “active sites” hypothesis and the “agglomerates” hypothesis (Jones and Price, 2006; Pilcer et al., 2012) (Figure 11).

The first hypothesis postulates that the carrier surface is characterized by the presence of sites that are more adhesive than others. These active sites may be caused by morphological defects (e.g., clefts and asperities), amorphous spots generated as a consequence of the production process (e.g., milling or spray drying) or regions with a different chemical composition (e.g., impurities). Fine lactose particles preferentially bind to areas with a more binding character, forcing drug particles to adhere to less

binding sites. In this way, during aerosolization, the detachment of drug particles from the carrier surface is easier, making a higher amount of API available for inhalation.
In the second case, the hypothesis is that, besides adhering to the surface of the carrier, drug particles form with fine lactose particles mixed agglomerates that are more easily aerosolized and dispersed.

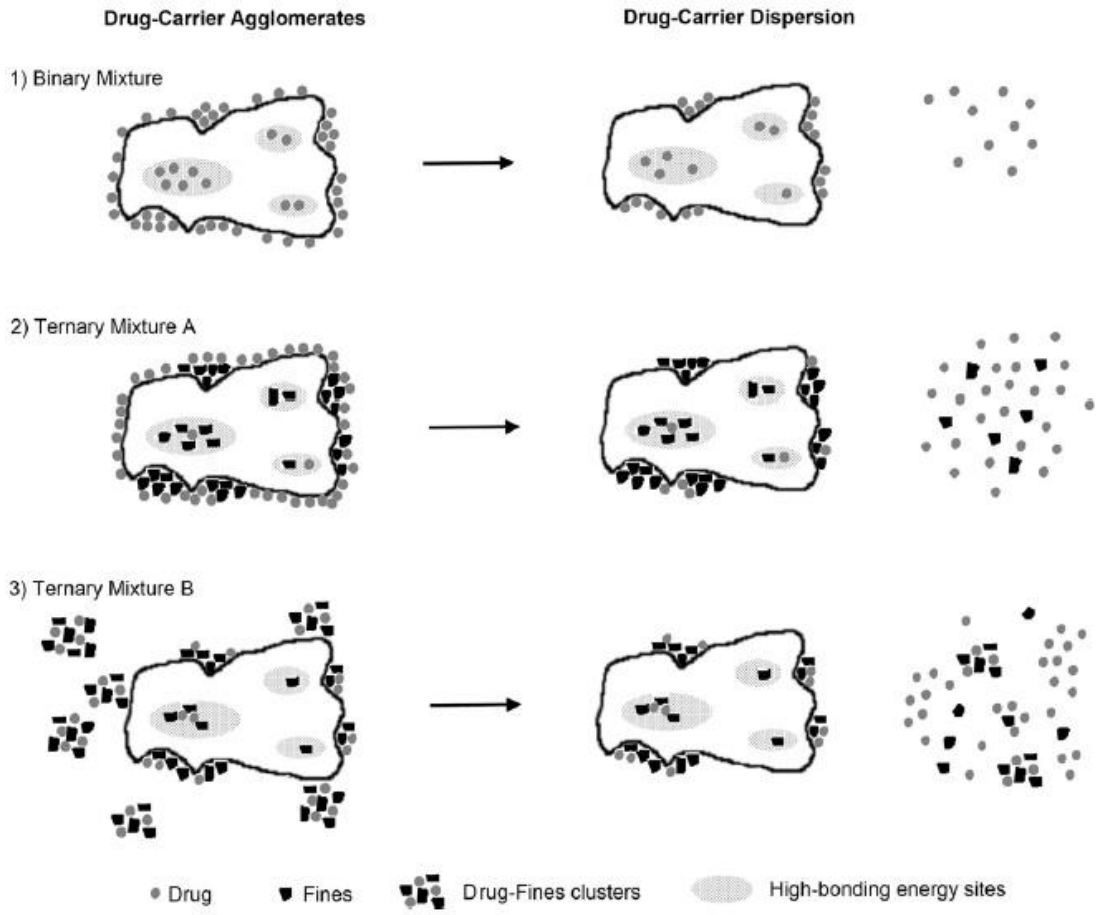


**Figure 11** Drug dispersion mechanisms in binary (1) and ternary (2, 3) mixtures ("active sites" theory (A), "multiplets" theory (B)) (Pilcer et al., 2012, reprinted with permission).

The influence of the order in which carrier, fine lactose particles and API are added to the formulation on the aerosolization performance supports the "active sites" hypothesis. In

fact, it has been reported that formulations produced by blending the coarse carrier and the fines before adding the drug gave higher FPD and FPF (Zeng et al., 1999).

However, also in this case literature reports discrepancies (Zeng et al., 2000d) and examples in which the mixing order resulted to be irrelevant on the deposition of the drug (Louey and Stewart, 2002; Lucas et al., 1998).

More recently, it has been shown that the relationship between blending order and fine particle delivery might be influenced by drug concentration and mixing time (Jones et al., 2010). This led the authors to suggest the "agglomerates" and the "tensile strength" hypotheses as more appropriate to explain the observed behaviour. The "tensile strength" hypothesis supposes that fine lactose particles enhance the cohesivity and the corresponding tensile strength of the bulk formulation, thus increasing the aerodynamic drag forces generated in the DPI device during inhalation. These increased forces, combined with the higher frequency of particle-particle and particle-wall collisions in the presence of fines, may result in improved performance (Shur et al., 2008).

In another study, Jones et al. investigated the dispersion mechanism of ternary mixtures by evaluating the relationship between interparticulate adhesion forces (expressed as drug-fines CAB ratios) and *in vitro* performance of a number of carrier-fines-drug combinations (Jones et al., 2008b). For adhesive drug-fines CAB ratios (i.e., < 1), increased adhesion between drug particles and fines likely led to the formation of larger agglomerates, which might be subject to greater deagglomeration forces during aerosolization, thus providing improved performance. On the other hand, when the API was more cohesive than adhesive to the fines (i.e., CAB ratio > 1), the mechanism responsible for the improved performance remained unclear, but it was speculated that it

might be related to an increased number of particle-particle collisions during the aerosolization.

The relevance of agglomerates formation was underlined also by Kinnunen et al. in a recent work (Kinnunen et al., 2015). The authors reported that increasing the content of lactose fines improved not only the FPF, but also the MMAD of budesonide, thus suggesting the deposition of drug in agglomerates. The formation and co-deposition of mixed agglomerates of lactose fines and budesonide was then confirmed by morphological and chemical (Raman) analysis of the material collected on stage 2 of the NGI (next generation impactor). Thus, agglomerates might also be small enough to contribute to the FPF without any detachment of drug particles, but in this case only the finest lactose fines will be efficient in improving DPI performance.

Finally, Grasmeijer et al. suggested that the effects of lactose fines may be explained by two new mechanisms in addition to those previously proposed (Grasmeijer et al., 2014). Lactose fines below a certain size may lower dispersion performance by increasing the effectiveness of press-on forces arising during the mixing process and/or through the formation of coherent fine particle networks containing the drug particles on the carrier surface. On the other hand, coarser lactose fines may weaken or prevent the formation of such coherent particle networks presumably by lowering their tensile strength.

In general, it can be concluded that the effect of added lactose fines on the dispersion performance of adhesive mixtures is likely the result of multiple mechanisms acting simultaneously. The balance between such mechanisms can be shifted by modifying a series of formulation and dispersion variables, such as the amount and the size of the added lactose fines, the blending method, the drug content and the inhalation flow rate.

## 1.4. Lactose and Process-Induced Solid-State Modifications

Thanks to its properties (it is non-toxic, cheap, readily available and relatively stable), lactose is a widespread excipient and the most commonly used carrier in dry powder formulations for inhalation.

Lactose is a disaccharide composed of a moiety of β-D-galactose linked to a moiety of α/β-D-glucose through a β1-4 glycosidic linkage. It may exist in two different forms, the α- and the β-form, which differ one from the other for the configuration of the anomeric carbon (C1) (Figure 12).

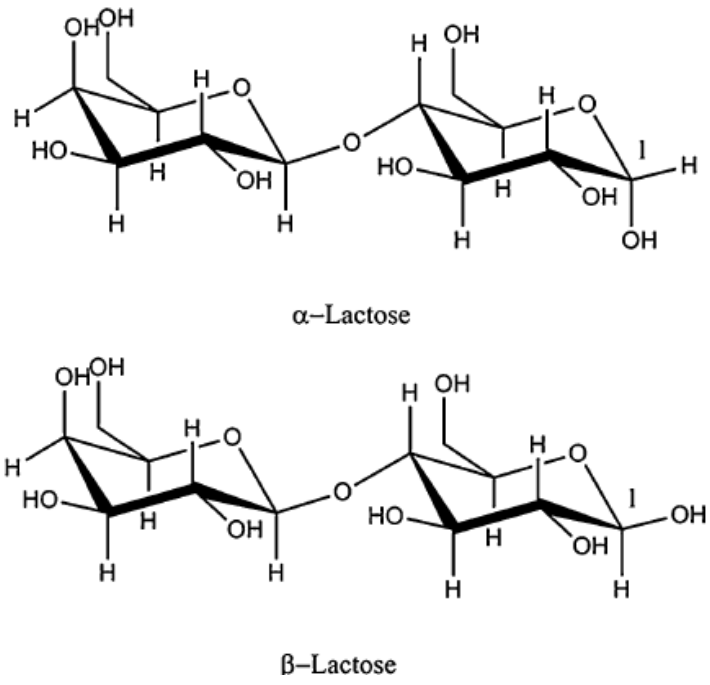


**Figure 12** Lactose α- and β-forms (Jawad et al., 2012, reprinted with permission, modified).

The interconversion between the two forms readily occurs in aqueous solution, where mutarotation takes place until an equilibrium (α/β 37:63 at neutral pH and room temperature) is reached (Jawad et al., 2012).

Moreover, lactose can be amorphous ($L_{am}$), with variable anomeric composition, or crystalline and exist in different polymorphs (or pseudopolymorphs).

Polymorphs are crystalline forms of the same pure substance characterized by different arrangements of the molecules in the crystal lattice. Pseudopolymorphs (or solvates) differ from each other for the presence of solvent molecules in the crystal lattice. Having a different crystalline structure, polymorphs exhibit different physico-chemical properties (e.g., solubility, melting point, stability, surface energy and hygroscopicity) and can be distinguished by using a variety of techniques such as differential scanning calorimetry (DSC), X-ray powder diffraction (XRPD), thermogravimetric analysis (TGA) and infrared spectroscopy (IR) (Carstensen, 2001; Craig and Reading, 2007).

Several lactose polymorphs are known, each of which has a specific crystalline structure: α-lactose monohydrate ($L\alpha \cdot H_2O$) (Beevers and Hansen, 1971; Fries et al., 1971; Smith et al., 2005), stable anhydrous α-lactose ($L\alpha_S$) (Platteau et al., 2005), hygroscopic anhydrous α-lactose ($L\alpha_H$) (Platteau et al., 2004), β-lactose (Lβ) (Garnier et al., 2002; Hirotsu and Shimada, 1974) and mixed α/β compounds with different stoichiometries (Earl and Parrish, 1983; Lefebvre et al., 2005).

As previously mentioned, α-lactose monohydrate is the most common lactose grade used in the inhalation field (Pilcer et al., 2012). It can be employed both as coarse carrier or fine particles. To produce these fine particles, inhalation lactose is often subject to unit processes such as micronization or spray drying which may alter its physico-chemical properties (Kou et al., 2012). Mutarotation and consequent variation of lactose anomeric composition have been reported as a possible consequence of milling (Otsuka et al., 1991) and spray drying processes (Jawad et al., 2012). Moreover, the formation of amorphous lactose upon milling/micronization is a known phenomenon well documented in the

literature (Briggner et al., 1994; Shariare et al., 2011; Willart et al., 2004; Young et al., 2007). Differently, the formation of other polymorphs, such as the α-anhydrous forms, has never been reported nor directly correlated to the above-mentioned unit processes.

However, it must be said that techniques such as XRPD and DSC, which are commonly used for the characterization of lactose, are not always capable to point out the solid-state changes induced by processing. This is due to the fact that the "new" forms of lactose might be generated in quantities that are considerably lower than the detection limit of the aforesaid techniques or to the fact that their distinctive signals could be partially or totally overlapped to those of the starting material, thus resulting hardly observable. Furthermore, certain behaviours still do not have an unambiguous interpretation. For example, considering the DSC trace of lactose, the presence of thermal events (peaks) in the region between the evaporation of crystalline water and the melting of lactose remains a source of different and sometimes conflicting interpretations (Figura and Epple, 1995; Kaialy et al., 2012b; Lerk et al., 1984a).

In this sense, a most suitable technique could be represented by dynamic vapour sorption (DVS). Few gravimetric methods that allow the quantification of amorphous material through the evaluation of vapour sorption/desorption isotherms have been described in the literature (Sheokand et al., 2014). Among these, the "residual weight" method was used by Buckton and Darcy (Buckton and Darcy, 1995) for an approximate quantification of low levels of amorphous lactose (down to 0.05% w/w). The method was based on the assumption that the final weight gain of a lactose sample is a consequence of the crystallization of the amorphous lactose into α-lactose monohydrate (Buckton, 1997). However, the application of this method to samples of lactose containing larger amounts of amorphous led to unsatisfactory results (Buckton and Darcy, 1999). This was due to

the fact that, in contrast with what was initially assumed, not all the amorphous lactose converts to α-lactose monohydrate, but both α- and β-lactose might be generated in different ratio during crystallization (Timmermann et al., 2006; Vollenbroek et al., 2010). Therefore, the amorphous content calculated according to the final weight gain was indefinitely underestimated.

In this context, it becomes clear the need for a reliable method able to identify and quantify all the different forms of lactose that might be generated in a sample as a consequence of a given process. These process-induced lactose phases are usually unwanted and must be seriously taken into account. In fact, since they mostly influence the surface energy and characteristics of lactose, they may result in a modified interaction with the drug and eventually affect the product performance and stability.

# *Aim of the Project*

# 2. AIM OF THE PROJECT

The aim of the present research project was to study the influence of lactose solid-state on the aerosolization performance of drug-carrier mixtures.

In particular, the modification of lactose physico-chemical properties induced by micronization was thoroughly investigated. Micronized lactose samples were characterized by proton nuclear magnetic resonance ($^1$H NMR), X-ray powder diffraction (XRPD) and differential scanning calorimetry (DSC) and compared with the starting material and some reference samples of different lactose forms: α-lactose monohydrate, hygroscopic anhydrous α-lactose, stable anhydrous α-lactose and amorphous lactose.

A new dynamic vapour sorption (DVS) method for the identification and quantification of all the α-lactose forms which may be generated as a consequence of the micronization process was developed and validated.

The effect of variable percentages of fine micronized lactose on the aerosolization performance of ternary mixtures containing salbutamol sulphate was considered. The stability of the mixtures stored under different conditions of temperature and relative humidity was evaluated as well.

Then, to study the effect of lactose solid-state on drug respirability, different lactose polymorphs (α-lactose monohydrate, stable anhydrous α-lactose and hygroscopic anhydrous α-lactose) were employed as carriers in binary mixtures with drugs possessing different hydrophilicity (salbutamol sulphate and budesonide).

The last part of the project was carried out at the Purdue University in West Lafayette (Indiana, USA) under the supervision of Prof. Teresa Carvajal and Prof. Rodolfo Pinal.

In an attempt to better understand the aerosolization performance of the studied drugs, inverse gas chromatography (IGC) was selected as technique to study the surface energetics of the components within the mixtures.

# *Materials and Methods*

# 3. MATERIALS AND METHODS

## 3.1. Materials

*Lactose*

Coarse α-lactose monohydrate ($d_{V50}$ = 91.7 μm) was supplied by Kerry (Ireland). Lacto-Sphere® MM50 (sieved α-lactose monohydrate, $d_{V50}$ = 53.1 μm) and Lacto-Sphere® MM3 (micronized lactose, $d_{V50}$ = 2.5 μm) were provided by Micro-Sphere SA (Switzerland).

*Active pharmaceutical ingredients (APIs)*

Salbutamol sulphate (SS, $d_{V50}$ = 2.7 μm) was supplied by Teva Pharmaceutical Industries (Israel). Salbutamol sulphate is a selective $\beta_2$ adrenergic receptor agonist used as a bronchodilator in the treatment of asthma and COPD and was chosen as model drug with hydrophilic characteristics (calculated $LogP_{ow}$ = 0.34[5]) (Figure 13).

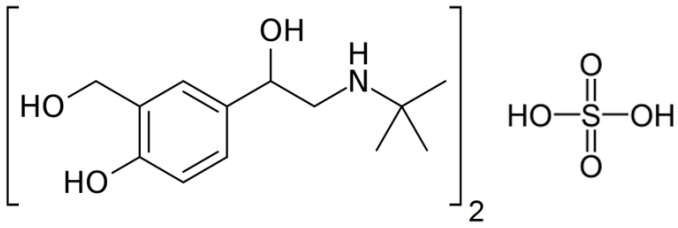


**Figure 13** Molecular structure of salbutamol sulphate.

Budesonide (BUD, $d_{V50}$ = 1.9 μm) was provided by Plantex Chemicals B.V. (Holland). Budesonide is an anti-inflammatory glucocorticoid used in the management of asthma

[5] http://www.chemspider.com/Chemical-Structure.36448.html, visited on January 22nd, 2016.

and was selected as model drug with lipophilic characteristics (calculated $LogP_{ow}$ = 2.91, measured $LogP_{ow}$ = 3.20 (Benet et al., 2011)) (Figure 14).

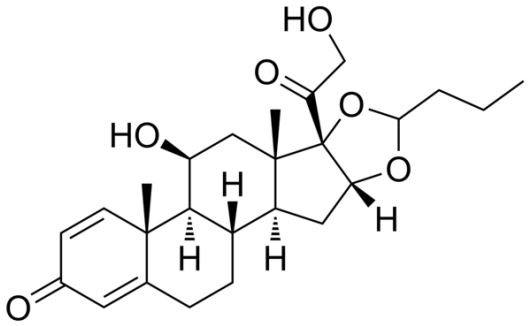


**Figure 14** Molecular structure of budesonide.

## 3.2. Methods

### 3.2.1. Micronization

The micronization of coarse α-lactose monohydrate was performed using a laboratory scale J-70 fluid jet micronizer (Tecnologia Meccanica, Italy). Nitrogen was used as fluid for the micronization. Samples with different particle size were obtained by varying three process parameters: the Venturi pressure $P_V$, the ring pressure $P_R$, and the feed rate $R_F$ (Figure 15).

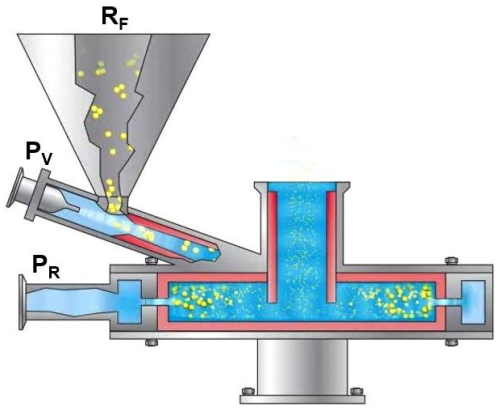


**Figure 15** Fluid jet micronizer scheme[6].

### 3.2.2. Preparation of Hygroscopic Anhydrous α-Lactose ($L\alpha_H$)

Hygroscopic anhydrous α-lactose was prepared based on the procedure reported by Garnier et al. (Garnier et al., 2002), which was partially modified. 7 grams of Lacto-Sphere® MM50 were placed with 250 glass beads (Ø = 3 mm) inside a 32 mL (14 mm internal diameter x 20 cm length) stainless steel column (Applied Separations, USA), kept in an oven at 25 °C for 2 hours under a dry nitrogen flow of 50 mL $min^{-1}$ and then heated at 120 °C for 9 hours under the same nitrogen flow. After production, $L\alpha_H$ has been always handled in a glove-box filled with dry nitrogen (RH < 5%) in order to prevent the possible conversion into α-lactose monohydrate.

[6] http://www.sturtevantinc.com/products/micronizer/, visited on January 22nd, 2016 (modified).

### 3.2.3. Preparation of Stable Anhydrous α-Lactose ($L\alpha_S$)

Stable anhydrous α-lactose was prepared by modifying the procedure reported by Kirk et al. (Kirk et al., 2007). 7 grams of Lacto-Sphere® MM50 were placed with 250 glass beads (Ø = 3 mm) inside a 32 mL (14 mm internal diameter x 20 cm length) stainless steel column (Applied Separations, USA), kept in an oven at 25 °C for 2 hours under a dry nitrogen flow of 50 mL $min^{-1}$ and then heated at 145 °C for 6 hours under the same nitrogen flow.

### 3.2.4. Preparation of Amorphous Lactose ($L_{am}$)

Different samples of amorphous lactose were produced by spray drying starting from 10% w/v aqueous solutions of α-lactose monohydrate. In order to obtain samples of amorphous lactose with different anomeric composition, the solutions were kept under stirring for variable times and at different temperatures: 20 minutes and 40 minutes in ice bath, 1 hour and 20 hours at 20 °C. Thereafter, they were spray dried using a Büchi Mini Spray Dryer B-290 (Büchi, Switzerland) set with an inlet temperature of 130 °C, an outlet temperature of 60 °C, a feed rate of 5 mL $min^{-1}$, a spray flow of 600 L $h^{-1}$ and an aspiration of 35 $m^3$ $h^{-1}$ (similar conditions were reported by Hill et al. (Hill et al., 1998)). The spray dried material was then stored under vacuum in a desiccator in the presence of $P_2O_5$ and handled in the above-mentioned dry glove-box (RH < 5%).

### 3.2.5. Proton Nuclear Magnetic Resonance ($^1$H NMR)

$^1$H NMR spectra were recorded in DMSO-$d_6$ at 25 °C using a Bruker AV400 spectrometer (Bruker, USA). Each measurement was performed at least in triplicate. The anomeric

composition of each sample of lactose was determined by integrating the peaks at δ = 6.3 ppm and δ = 6.7 ppm, corresponding to the protons of the hydroxyl group at carbon C1 in the α- and β-anomer, respectively (Jawad et al., 2012). Spectra were processed using MestReNova software (Mestrelab Research, Spain). An apodization of 0.2 Hz was applied and spectra were manually phase corrected prior to automatic baseline correction and final peak integration.

### 3.2.6. X-Ray Powder Diffraction (XRPD)

X-ray diffraction patterns on powder were recorded on a MiniFlex diffractometer (Rigaku, Japan) using Cu $K_\alpha$ radiation (λ= 1.5418 Å) generated with 30 kV. The samples of lactose powder were transferred into the sample holder until it was completely full and then pressed with a glass slide in order to obtain a flat and homogeneous surface. The goniometer was set at a scanning rate of 1.5 ° $min^{-1}$ (step size = 0.05 °) over the $2\theta$ range 2-40 °. Each measurement was carried out at least in triplicate. The degree of crystallinity, $C$, was calculated for each sample as:

$$C = R_x \times 100 \qquad [2]$$

where $R_x$ is the ratio of the area under the crystalline peaks (calculated in the $2\theta$ range 5-30 ° following a background subtraction according to the method described by Sonneveld and Visser (Sonneveld and Visser, 1975)) to the total area (calculated in the $2\theta$ range 5-30 °) (Shah et al., 2006). Areas were determined using the Integral Intensity Calculation program of MiniFlex Standard Software (Rigaku).

### 3.2.7. Differential Scanning Calorimetry (DSC)

DSC measurements were performed using an Indium calibrated (onset of melting $T_m$ = 156.48 °C, enthalpy of melting $\Delta H_m$ = -28.60 J $g^{-1}$) DSC 821e instrument (Mettler Toledo, Switzerland) driven by STARe software (Mettler Toledo). DSC traces were recorded by placing accurately weighed quantities (6-12 mg) of powder samples in a 40 μL Aluminium pan which was then sealed and pierced twice. Scans were performed between 25 and 250 °C at a scanning rate of 10 °C $min^{-1}$ under a purging nitrogen atmosphere (100 mL $min^{-1}$). Each measurement was carried out at least in triplicate. Data relevant to the observed thermal events were reported as peak temperatures.

### 3.2.8. Dynamic Vapour Sorption (DVS)

DVS studies were performed with an Aquadyne DVS-2 (Quantachrome Instruments, USA) using a gravimetric approach. The instrument was calibrated at 25 °C, 50% RH using a 200 mg standard weight. The samples of lactose (about 30 mg) were analysed at 25 °C by measuring the water vapour sorption in the 5-90% RH range (step size = 5% RH). The analysis was preceded by a purging step at 60 °C, 1% RH in order to remove any surface water from the sample. The transition from one step to the next occurred when the rate of weight variation was lower than 0.001% $min^{-1}$ and in any case not earlier than 30 minutes from the beginning of the step.

### 3.2.9. Particle Size Determination

The particle size distribution of lactose samples and APIs was determined by laser light diffraction using a Spraytec analyser (Malvern, UK). Two different procedures were adopted.

In the first case, a supersaturated solution of lactose in ethanol was prepared adding 5 grams of lactose to 1 L of ethanol (96% v/v). The solution was stirred overnight and then filtered under vacuum through a nylon membrane filter (0.45 µm, Ø 47 mm, Whatman®, GE Healthcare Life Sciences, UK). The obtained solution was used as dispersing liquid for the analysis. 100 mg of each sample were dispersed in 10 mL of solvent and sonicated for 5 minutes before being analysed. Each measurement was repeated three times with an 8% obscuration threshold.

To determine the particle size distribution of the APIs, cyclohexane was chosen as dispersing liquid. 10 mg of drug were suspended in a 0.1% w/v solution of Span® 85 in cyclohexane and sonicated for 5 minutes before being analysed. Each measurement was repeated three times using an 8% obscuration threshold.

### 3.2.10. Scanning Electron Microscopy (SEM)

Morphology and surface roughness of lactose carriers were visually assessed by scanning electron microscopy using a FESEM SUPRA™ 40 (Carl Zeiss, Germany). Each powder sample was placed on a conductive sample holder previously covered with a double-sided conductive carbon tape so as to allow the dispersion of the charge. Particles in excess were removed by a gentle flow of nitrogen. The samples were analysed under high

vacuum conditions and the images were collected at different magnifications using a voltage of 1.5 or 2.0 kV.

### 3.2.11. Preparation of Adhesive Mixtures

Mixtures containing the 1% w/w of the selected API were blended with a Turbula® T2A shaker-mixer (WAB, Switzerland) at 30 rpm using a stainless steel vessel (internal volume = 240 mL, internal diameter = 5 cm, height = 12 cm) which was grounded to prevent the accumulation of electrostatic charges.

*Ternary mixtures*

6 grams of each formulation were prepared according to a four steps procedure:

- mixing of coarse and fine lactose for 30 minutes (*pre-mix*);
- mixing of 0.6 grams of *pre-mix* with the API for 30 minutes;
- addition of 1.8 grams of *pre-mix* followed by a 30 minutes mixing step;
- addition of the remaining portion of *pre-mix* and mixing for 1 hour.

*Binary mixtures*

6 grams of each formulation were prepared following a three steps procedure:

- mixing of 0.6 grams of carrier with the API for 30 minutes;
- addition of 1.8 grams of carrier followed by a 30 minutes mixing step;
- addition of the remaining portion of carrier and mixing for 1 hour.

### 3.2.12. UV Analysis of Salbutamol Sulphate

The quantitative analysis of salbutamol sulphate was performed by UV spectroscopy. Measurements were carried out with a V-570 UV-Vis/NIR spectrophotometer (Jasco, USA). The absorbance of each sample was determined at $\lambda$ = 224 nm using quartz cuvettes with optical path of 1 cm. For each sample three quantitative determinations were carried out, each of which was obtained as the average of ten consecutive readings. The analytical method was validated as regards the linearity of the response (absorbance *vs* concentration) in the concentration range 5-64 μg $mL^{-1}$ using water as solvent, limit of detection (LOD = 0.57 μg $mL^{-1}$) and limit of quantification (LOQ = 1.91 μg $mL^{-1}$).

Another calibration curve (absorbance *vs* concentration) was built to evaluate the UV response of the capsules employed in the *in vitro* deposition tests. The linearity of the response was assessed in the concentration range 2-14 mg $mL^{-1}$ (LOD = 0.57 mg $mL^{-1}$, LOQ = 1.89 mg $mL^{-1}$) using water as solvent.

### 3.2.13. HPLC Analysis of Budesonide

The quantitative determination of budesonide was performed by HPLC. A system composed of two LC-10AT VP pumps (Shimadzu, Japan), a SPD-M10A VP diode array detector (Shimadzu), a CTO-10AS VP oven column (Shimadzu) and a Waters 717 plus autosampler (Waters, USA) was used. The analysis was carried out at 25 °C using a Nova-Pak C-18 column (4 μm, 3.9 mm x 150 mm, Waters). Budesonide-containing solutions were isocratically eluted at a flow of 0.6 mL $min^{-1}$ employing an acetonitrile/water (6:4 v/v) solution as mobile phase. An injection volume of 50 μL, a time of 6 minutes and a wavelength of 254 nm were set for the analysis. The analytical method was validated in

terms of linearity of the response (peak area *vs* concentration) in the concentration range 0.3-26.6 μg $mL^{-1}$ (LOD = 0.026 μg $mL^{-1}$, LOQ = 0.087 μg $mL^{-1}$) using an acetonitrile/water (6:4 v/v) solution as solvent.

### 3.2.14. Homogeneity Test

The homogeneity of the prepared mixtures was checked at the end of the mixing procedure. For each formulation, five samples (20 mg each) were collected from different spots of the powder bed. Each sample was dissolved in 10 mL of an appropriate solvent (water in the case of salbutamol sulphate, an acetonitrile/water (6:4 v/v) solution in the case of budesonide) and the quantification of the drug was performed. Homogeneity was assumed at a coefficient of variation (calculated as the percentage of the ratio between standard deviation and mean value on the five measurements) lower than 5%.

### 3.2.15. *In Vitro* Aerodynamic Assessment

*In vitro* aerodynamic assessment was performed using a next generation impactor (NGI, Copley Scientific, UK) equipped with a pre-separator. In order to control particle rebound, the cups corresponding to the first seven stages of the impactor were coated with a suitable filming solution and then allowed to dry prior to use. A 1% w/w solution of glycerine in methanol was used when mixtures containing salbutamol sulphate were tested. Differently, a 1% w/v solution of Span® 85 in cyclohexane was used in the case of mixtures containing budesonide. The terminal stage (micro-orifice collector, MOC) was fitted with a glass fibre filter (Type A/E, Pall Corporation, USA). The central cup of

the pre-separator was filled with 15 mL of water in the case of salbutamol sulphate and with an acetonitrile/water (6:4 v/v) solution in the case of budesonide.

After completing the assembly, the NGI was connected to a VP 1000 vacuum pump (Erweka, Germany) and the flow rate through the impactor was measured by a mass flowmeter (model 3063, TSI, USA).

A low resistance single-dose DPI, Turbospin® #2 (PH&T, Italy), was chosen as device. For each mixture, ten Quali-V® capsules size 2 (Qualicaps® Europe, Spain) were filled with 20.0 ± 0.1 mg of powder, introduced in the inhaler device and finally pierced. Once connected the device to the impactor through an airtight rubber mouth, the vacuum pump was activated at a flow of 70 L $min^{-1}$ for 3.4 seconds so that 4 L of air were drawn through the apparatus (Ph. Eur. 8.0, 2.9.18). Ten consecutive aerosolizations were performed for each mixture. At the end of the deposition experiment, the NGI was disassembled and two different procedures were adopted depending on the API under examination.

Salbutamol sulphate deposited on each stage of the impactor was recovered with aliquots of water which were finally transferred into volumetric flasks of adequate volume. The obtained solutions were filtered through a cellulose acetate syringe filter (porosity 0.45 µm, GVS Filter Technology, USA) before being analysed. A volumetric flask named *device* was used to collect the salbutamol sulphate remained in the Turbospin® device and the capsules which were dissolved in water at the end of the experiment in order to ensure complete recovery of the active ingredient. Therefore, in this case, the absorbance initially recorded was corrected by subtracting the contribution due to the absorbance of the Quali-V® capsules.

Budesonide was recovered from each stage of the impactor with appropriate volumes of an acetonitrile/water (6:4 v/v) solution. Before being transferred into vials, the solutions

were filtered through a regenerated cellulose syringe filter (porosity 0.45 μm, Analytical Technology, Italy).

All the mixtures were tested in triplicate immediately after preparation. Their performance was evaluated by calculating:

- the emitted dose (ED), obtained as the sum of the portions of drug recovered from the mouthpiece adapter, the induction port, the pre-separator and all the stages of the impactor and expressed in μg;
- the fine particle dose (FPD), namely the quantity of drug with a cut-off diameter lower than 5 μm, calculated by interpolation according to the European Pharmacopoeia (Ph. Eur. 8.0, 2.9.18) and expressed in μg;
- the fine particle fraction (FPF), calculated as the ratio of the FPD to the ED and expressed as percentage.

### 3.2.16. Inverse Gas Chromatography (IGC)

The surface energy of lactose carriers and APIs was measured using an IGC system (Surface Measurement Systems, UK). Powder samples ranging from 0.3 to 1.4 grams were weighed inside pre-silanized glass columns (30 cm length, 6 mm outer diameter x 4 mm internal diameter, Surface Measurement Systems), plugged with glass wool and tapped for 10 minutes with a column packing device (Surface Measurement Systems). Each sample was purged under a 10 mL $min^{-1}$ helium flow first at 40 °C, 0% RH for 2 hours, then at 30 °C, 0% RH for 2 hours prior to measurement. Analyses to determine dispersive surface energy were performed at 60% and 0% RH (25 °C, 10 mL $min^{-1}$ gas flow rate). Specific surface energy was evaluated at 60% RH (25 °C, 10 mL $min^{-1}$ gas

flow rate). Retention times of non-polar probes (*n*-alkane C6-C10 series) and polar probes (ethyl acetate, acetone, acetonitrile and chloroform) were determined at infinite dilution (0.03 $p/p^0$) using a flame ionization detector. Methane was used to calculate dead volumes. Measurements were performed at least in triplicate.

### 3.2.17. Statistical Analysis

Statistical evaluation of the collected data was performed with Microsoft® Excel® software. Data were expressed as mean ± standard deviation. Regression analysis of DVS data was carried out with the method of least squares. Significance for both slope and intercept was accepted at 95% (t-test, two tails).

# *Results and Discussion*

# 4. RESULTS AND DISCUSSION

## 4.1. Effect of Micronization on Lactose Solid-State

### 4.1.1. Micronization

Two samples of micronized lactose were produced by varying the process parameters (i.e., Venturi pressure $P_V$, ring pressure $P_R$ and feed rate $R_F$) so as to obtain a different particle size. The experimental matrix and the resulting particle size distributions are reported in Table 1.

**Table 1** Setting of the process parameters for the production of micronized lactose samples and resulting particle size distribution parameters.

| Sample | $P_V$ (bar) | $P_R$ (bar) | $R_F$ (kg $h^{-1}$) | $d_{V10}$ (µm) | $d_{V50}$ (µm) | $d_{V90}$ (µm) |
|---|---|---|---|---|---|---|
| Lactose-7 | 7 | 6 | 2 | 1.3 | 6.5 | 14.5 |
| Lactose-2 | 10 | 10 | 1 | 0.5 | 2.1 | 5.2 |

As expected, the greatest size reduction was achieved by applying higher pressures and lower feed rate.

### 4.1.2. Characterization of the Produced Samples

The starting material (coarse α-lactose monohydrate) and all the produced lactose samples were characterized with different techniques in order to evaluate the potential influence of the micronization process on the physico-chemical properties of lactose. Furthermore, four additional lactose samples were characterized with the same techniques in order to be used as reference materials: Lacto-Sphere® MM50 (employed as reference for α-

lactose monohydrate, Lα·$H_2O$), stable anhydrous α-lactose ($L\alpha_S$), hygroscopic anhydrous α-lactose ($L\alpha_H$) and amorphous lactose ($L_{am}$).

## Proton Nuclear Magnetic Resonance ($^1$H NMR)

The anomeric composition of each lactose sample was determined through $^1$H NMR by applying the method described by Jawad et al. (Jawad et al., 2012) (see section 3.2.5). The obtained results are reported in Table 2.

**Table 2** Percentage of β-form in the analysed lactose samples. For $L_{am}$, the time and the temperature at which the feed solution was kept under stirring before being spray dried are reported in brackets.

| Sample | β-form (%) |
|---|---|
| Lα·$H_2O$ | 0.9 ± 0.2 |
| $L\alpha_S$ | 5.1 ± 0.2 |
| $L\alpha_H$ | 6.1 ± 0.4 |
| $L_{am}$ (1 hour, 20 °C) | 46.4 ± 0.9 |
| Starting material | 1.6 ± 0.1 |
| Lactose-7 | 1.4 ± 0.1 |
| Lactose-2 | 1.7 ± 0.1 |

While Lα·$H_2O$ was composed almost exclusively of α-lactose, in the case of $L\alpha_S$ and $L\alpha_H$, thermal dehydration probably led to a disordered intermediate state which allowed the formation of small quantities of β-form (Garnier et al., 2002). The considerable amount of β-form exhibited by $L_{am}$ was, instead, a direct consequence of the mutarotation that occurred in the feed solution before/during the spray drying process.

As regards the effect of micronization, no significant variation of β-lactose content between micronized samples and the starting material was observed (t-test, $p > 0.05$). Indeed, both the produced samples contained a negligible amount of β-lactose.

## X-Ray Powder Diffraction (XRPD)

The reference samples were characterized by XRPD. The relevant diffraction patterns are shown in Figure 16.

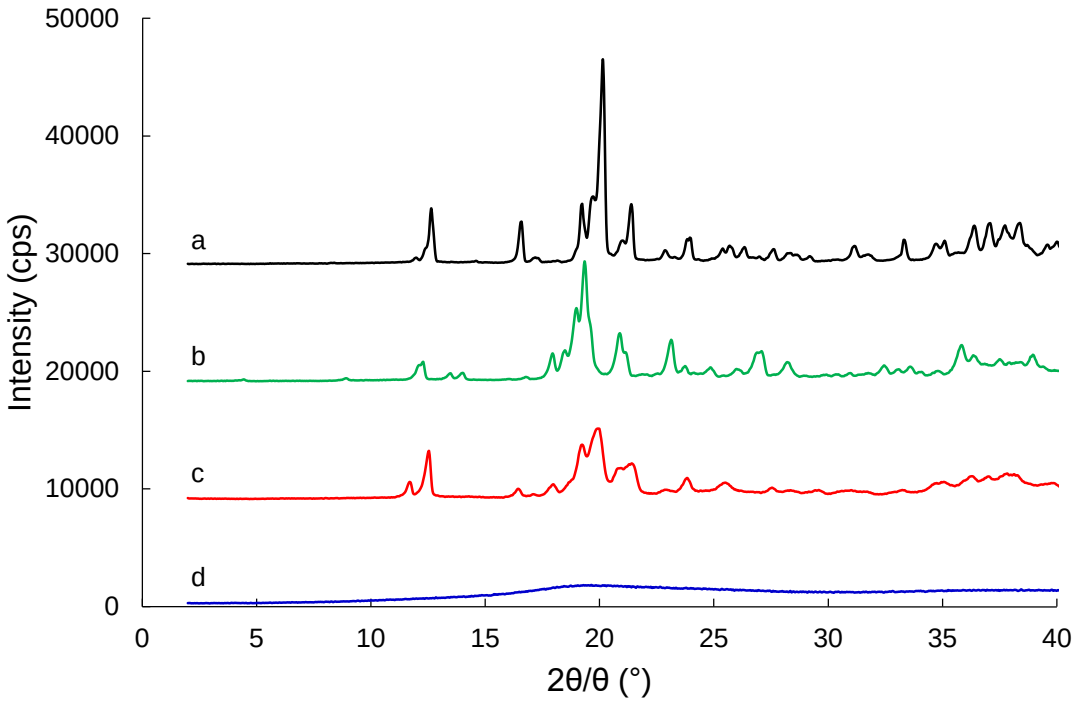


**Figure 16** X-ray diffraction patterns on powder of the three polymorphs of α-lactose (Lα·$H_2O$ (a), $L\alpha_S$ (b) and $L\alpha_H$ (c)) and $L_{am}$ (d).

While $L_{am}$ exhibited a diffuse halo, the diffractograms of the polymorphs of α-lactose showed characteristic peaks of diffraction that allowed their identification (Kirk et al., 2007). Both the diffractograms of $L\alpha_S$ and $L\alpha_H$ did not show the distinctive peak of β-lactose at 10.5 ° 2$\theta$ (Kirk et al., 2007). This could be due to the fact that the amount of β-lactose in the samples was too low to be detected. A possible explanation is that β-lactose was not present as pure crystallite, but β-lactose molecules could have substituted for some α-lactose molecules in $L\alpha_S$ and $L\alpha_H$ (Platteau et al., 2004). In other words,

mutarotation during thermal dehydration presumably resulted in the formation of mixed α/β lactose crystals, rather than pure crystals of α- and β-lactose.

Figure 17 shows the diffraction patterns of the samples of micronized lactose in comparison with that of the starting material.

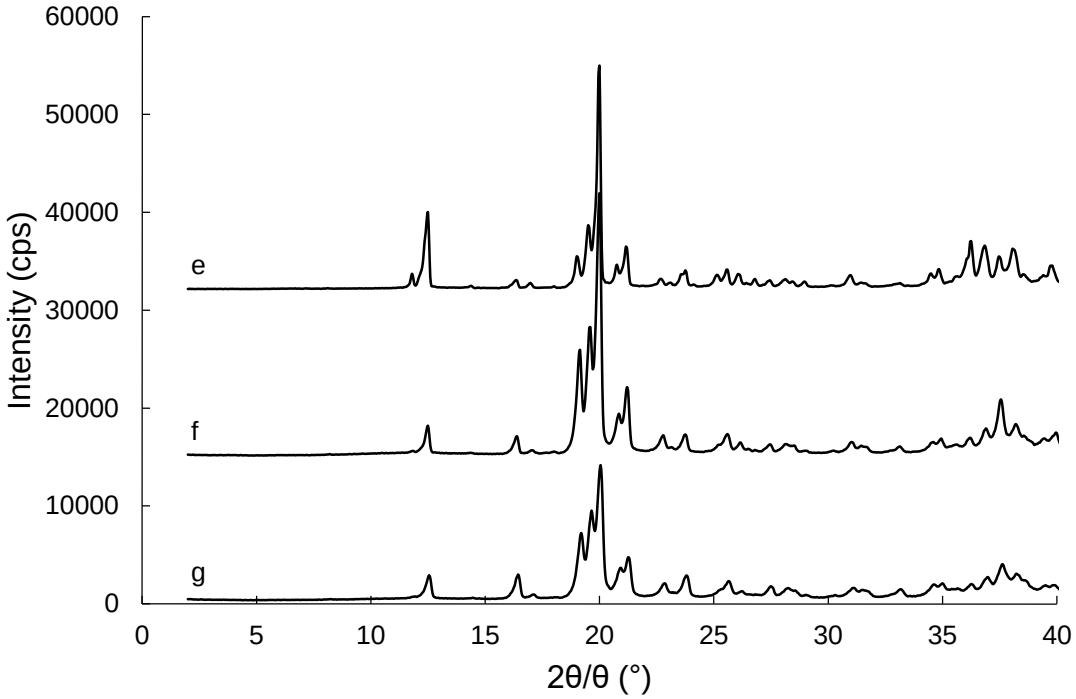


**Figure 17** X-ray diffraction patterns on powder of the samples of micronized lactose (Lactose-7 (f) and Lactose-2 (g)) compared to that of the starting material (e).

The diffractograms were very similar to each other and exhibited the characteristic pattern of α-lactose monohydrate. In agreement with $^{1}$H NMR data, no β-lactose was detected. Since the distinctive peaks of each polymorph of α-lactose lie almost in the same regions of the diffraction pattern, it was not possible to evaluate the presence of polymorphs different from the α-monohydrate. In addition to that, it must be considered that the amount of amorphous/anhydrous lactose potentially generated as a consequence of the micronization process could be lower than the detection limit of the technique, which is typically around 10% in the case of XRPD (Saleki-Gerhardt et al., 1994).

Nevertheless, some differences in terms of degree of crystallinity (see section 3.2.6) were identified (Table 3).

**Table 3** Degree of crystallinity, $C$, of the samples of micronized lactose compared to that of the starting material. $\Delta C$ represents the percent variation in the cristallinity of the micronized samples with respect to the starting material.

| Sample | $C$ | $\Delta C$ (%) |
|---|---|---|
| Starting material | 71 ± 2 | - |
| Lactose-7 | 63 ± 1 | -11 |
| Lactose-2 | 56 ± 1 | -20 |

The obtained values were not intended to be considered as absolute values of crystallinity, but have been used for comparative purposes (Ph. Eur. 8.0, 2.9.33). In fact, the degree of crystallinity progressively decreased with the reduction of the particle size. According to the common knowledge, this could be attributed to the presence of a certain amount of amorphous lactose generated by the progressively stronger micronization conditions (Briggner et al., 1994; Shariare et al., 2011). However, the micronization process may also have induced some anisotropic lattice distortions, thus generating a certain amount of hygroscopic anhydrous α-lactose which, compared to α-lactose monohydrate, has a lower crystallinity (Figura and Epple, 1995; Garnier et al., 2008).

## Differential Scanning Calorimetry (DSC)

The solid-state of all the samples of lactose was further evaluated by DSC. Figure 18 shows the DSC traces of the reference lactose samples.

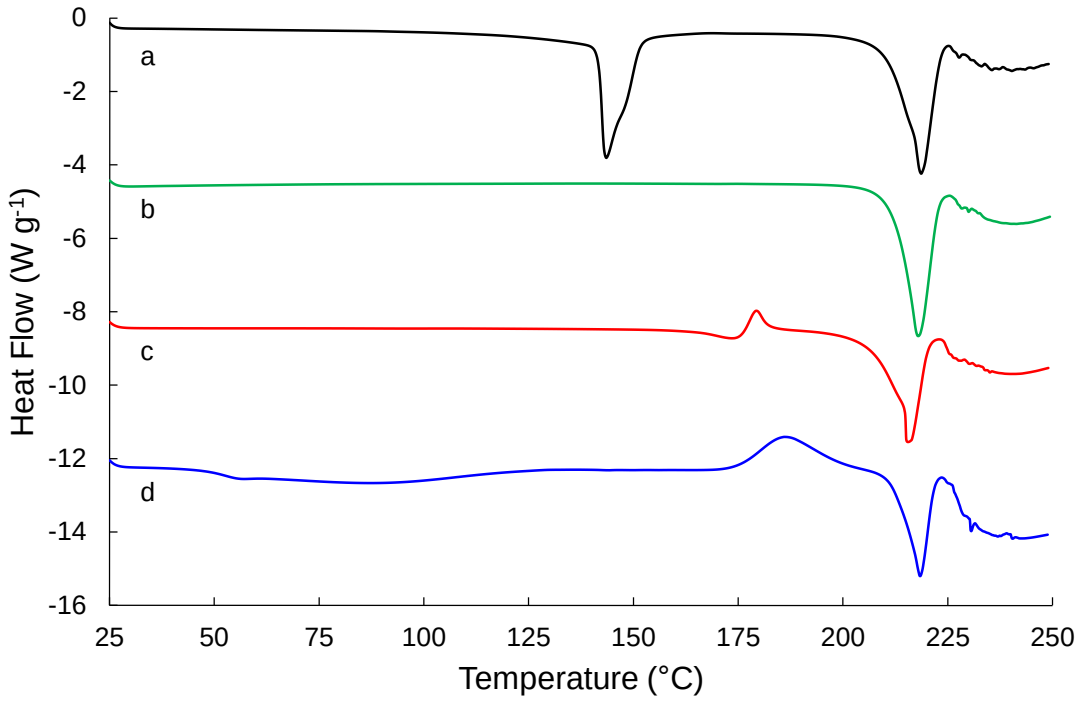


**Figure 18** DSC traces of the three polymorphs of α-lactose (Lα·$H_2O$ (a), L$\alpha_S$ (b) and L$\alpha_H$ (c)) and $L_{am}$ (d).

The DSC trace of Lα·$H_2O$ showed two endothermic peaks, the first at 143.4 ± 0.3 °C caused by the evaporation of the water of crystallization, the second at 218.7 ± 0.2 °C corresponding to the melting of lactose before decomposition.

In the DSC trace of L$\alpha_S$ the endothermic peak due to the evaporation of crystalline water was, obviously, no longer visible and the melting of lactose occurred at 218.0 ± 0.1 °C.

The DSC curve of L$\alpha_H$ showed some differences compared to the previous ones. Once again, the peak corresponding to the evaporation of crystalline water was missing, but the final melting of lactose (215.8 ± 0.9 °C) was preceded by two thermal events. The first endothermic peak (173.4 ± 0.6 °C) can be attributed to the melting of the metastable anhydrous α-lactose, whereas the subsequent exothermic transition (179.4 ± 0.3 °C) was ascribed to the crystallization of an α/β-lactose mixture (Garnier et al., 2002; Lerk et al., 1984a). L$\alpha_H$ is thermodynamically unstable and tends to reconvert into Lα·$H_2O$ with a

kinetics strongly dependent on the relative humidity of the storage environment (Kirk et al., 2007). Its DSC trace will vary accordingly, showing the progressive decrease of the above-described additional peaks and the concomitant increase of the endothermic peak related to the presence of crystalline water.

The DSC trace of $L_{am}$ was characterized by the presence of a broad exothermic peak (186.4 ± 0.5 °C) due to the crystallization of amorphous lactose before the final melting (217.7 ± 0.7 °C).

The samples of lactose produced by micronization were analysed by DSC and compared to the starting material (Figure 19).

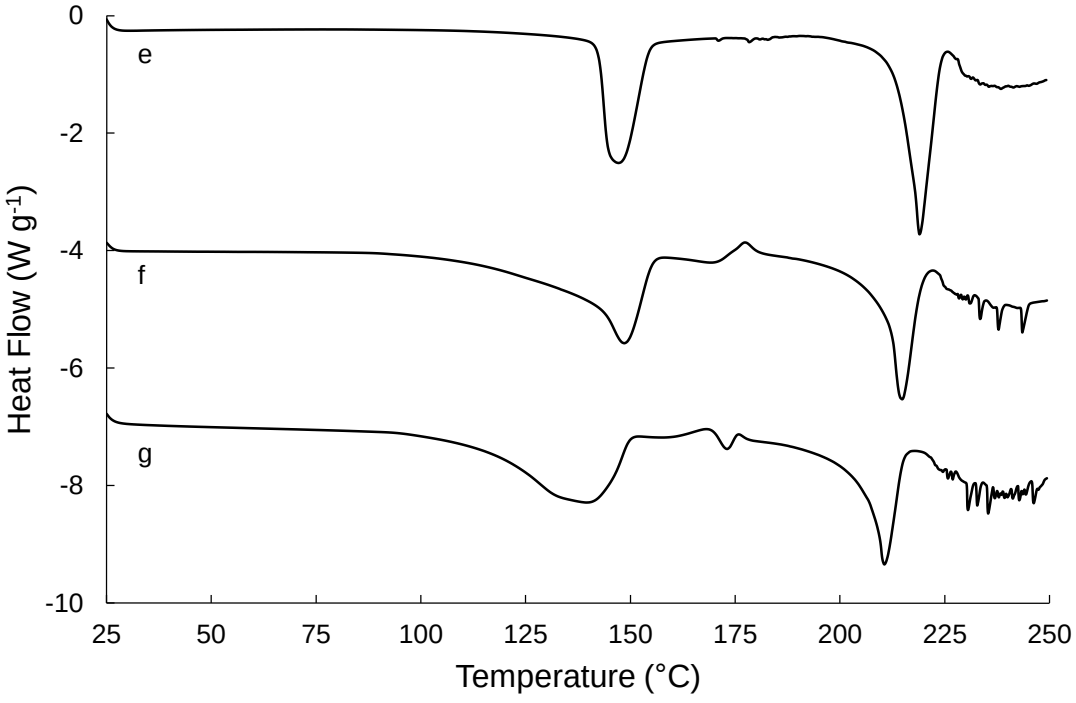


**Figure 19** DSC traces of the samples of micronized lactose (Lactose-7 (f) and Lactose-2 (g)) compared to that of the starting material (e).

It is worth to point out that the DSC curve of the starting material (coarse $L\alpha \cdot H_2O$) was not precisely superimposable to that of the reference $L\alpha \cdot H_2O$ (Figure 18, curve a), despite they were the same material, with the reference exhibiting only a lower particle size. This

observation further evidences the previously presented difficulties related to the use of DSC for the analysis of lactose for inhalation.

The DSC curves of the micronized samples showed additional transitions in the region between the evaporation of crystalline water and the melting of lactose. These thermal events were representative of the presence of "new" forms of lactose generated mainly by mechanical stress stemming from micronization. As a matter of fact, the micronization conditions generated with the used fluid jet micronizer were such that the thermal stress was minimized due to the use of cold nitrogen (coming from a liquid nitrogen tank) as fluid for the micronization.

In particular, the thermal events exhibited by Lactose-7 (a first endothermic peak at 169 °C and a second exothermic peak at 177 °C) were comparable to those observed for $L\alpha_H$, thus revealing the presence of this polymorph in the sample.

The DSC trace of Lactose-2 was more complicated and not straightforwardly correlated to any of the DSC traces reported in Figure 18. In this case, the region between the loss of crystalline water and the melting of lactose was characterized by the presence of three additional peaks. Taking into consideration the literature and the data obtained by XRPD, the first exothermic peak (168 °C) was attributed to the crystallization of a small amount of amorphous lactose (Gombás et al., 2002; Hill et al., 1998; Lerk et al., 1984b), while the other endothermic (173 °C) and exothermic (176 °C) transitions were indicative of the presence of $L\alpha_H$ (Garnier et al., 2002; Garnier et al., 2008; Lerk et al., 1984a).

Literature offers a variety of interpretations (Figura and Epple, 1995; Kaialy et al., 2012b; Lerk et al., 1984a) about the assignment of these peaks although a case analogous to that of Lactose-2 has never been reported. Therefore, to shed some light on this point, a further investigation of the thermal behaviour of the different forms of lactose was performed.

Three physical mixtures of $L\alpha_H$ and $L_{am}$ (mixture A 1:3, mixture B 1:1, mixture C 3:1) were prepared and analysed by DSC. The aim was to obtain a DSC trace as similar as possible to that of Lactose-2 in order to correlate each of the aforementioned peaks to the presence of a specific form of lactose. The mixtures were prepared in a dry glove-box weighing the amounts of lactose directly inside the Aluminium pan used for the analysis. The DSC traces obtained for the three mixtures are shown in Figure 20.

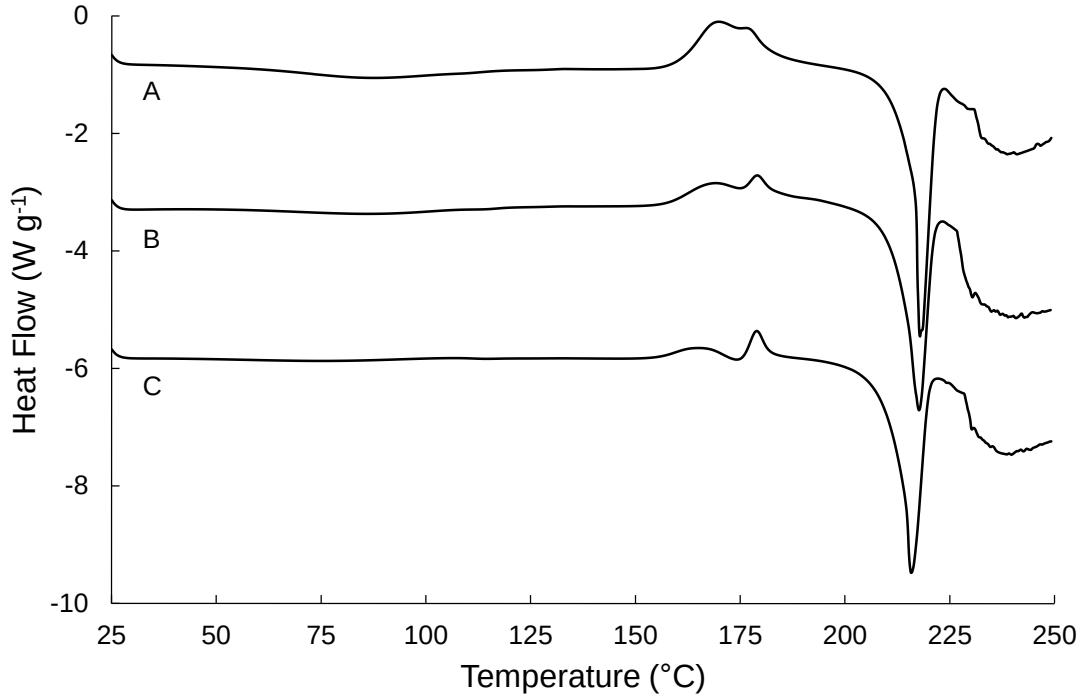


**Figure 20** DSC traces of the physical mixtures of $L\alpha_H$ and $L_{am}$ (A 1:3 mixture, B 1:1 mixture, C 3:1 mixture).

As the amount of $L_{am}$ in the physical mixture was reduced, a decrease in the intensity of the first exothermic peak was observed. On the contrary, with the increase of the amount of $L\alpha_H$, the endothermic and exothermic transitions indicative of the presence of this polymorph became more visible. The peak corresponding to the crystallization of the amorphous lactose shifted from 186 °C (Figure 18, curve d) to 168 °C likely because, in

this latter case, the crystallization was favoured by the presence of the crystals of hygroscopic anhydrous α-lactose which acted as crystallization drivers.

Considering the thermal events that preceded the final melting of lactose, the DSC traces of mixture B and mixture C were definitely similar to that of Lactose-2 (Figure 19, curve g) and thus confirmed the presence of both amorphous and hygroscopic anhydrous α-lactose in the sample of micronized lactose produced under more stressed conditions.

Unfortunately, the partial overlapping of the peaks related to the presence of hygroscopic anhydrous α-lactose and amorphous lactose prevents the quantification of these forms when they are simultaneously present in a given sample. Even experiments performed at different heating rates were unsuccessful in achieving a better resolution of these peaks.

## 4.2. A New DVS Method for the Quantification of α-Lactose Forms

Due to the limitations shown by XRPD and DSC, dynamic vapour sorption (DVS) was chosen as the technique to develop a new method for the identification and quantification of the different forms of lactose that might be generated as a consequence of the micronization process.

The selected reference samples ($L\alpha \cdot H_2O$, $L\alpha_S$, $L\alpha_H$ and $L_{am}$) were subject to vapour sorption isotherms in the 5-90% RH range. The obtained DVS profiles were carefully analysed in an attempt to find for each form of lactose a distinctive behaviour to be used for its identification. Similarly to what described by Burnett et al. for the quantification of amorphous lactose (Burnett et al., 2009), the idea was to correlate the weight variation at a certain value of relative humidity to the amount of a specific lactose form.

Given the negligible amount of β-form contained in the starting material and considering that micronization did not induce mutarotation (as proven by $^1$H NMR data), β-lactose was not included in the set of reference lactose forms. However, it must be underlined that an accurate evaluation of the behaviour of lactose samples containing a certain amount of β-form would still be hardly achievable. In fact, those samples might consist of mixed α/β lactose crystals, rather than pure crystals of α- and β-lactose and exhibit different vapour sorption depending on their stoichiometry. In the light of these considerations, the lactose β-form contained in $L\alpha_S$ and $L\alpha_H$ ($\leq$ 6.1%) was neglected as well. Reference $L\alpha_S$ and $L\alpha_H$ were treated as pure α-lactose forms, thus introducing a small approximation in the method. Despite its anomeric composition, the sample of amorphous lactose containing 46% β-form was still employed as reference sample for the amorphous α-form. To do so, three additional samples of amorphous lactose with variable

anomeric composition were prepared and submitted to DVS analyses in order to draw a correction factor which allowed to evaluate the behaviour of pure α-lactose samples. Figure 21 shows the DVS profiles recorded for the reference lactose forms.

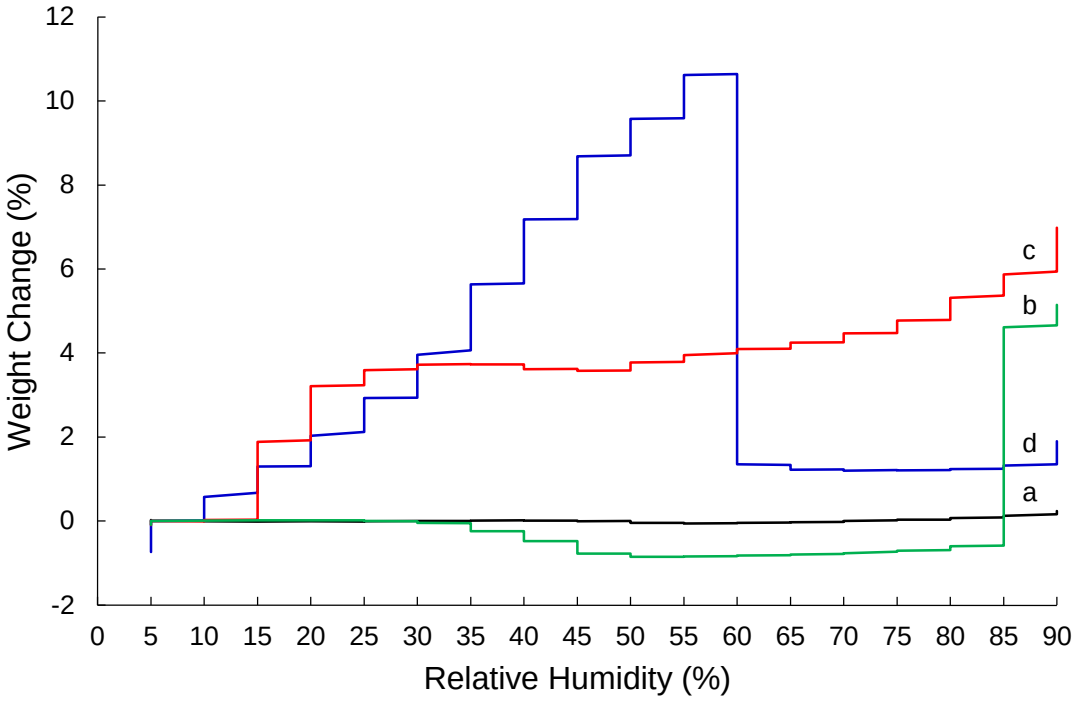


**Figure 21** DVS profiles (% weight change *vs* RH) of Lα·$H_2O$ (a), $L\alpha_S$ (b), $L\alpha_H$ (c) and $L_{am}$ (d).

While Lα·$H_2O$ essentially did not show water sorption in the RH range tested, the other forms of lactose were characterized by water sorption of variable extent in specific regions of the DVS profile. In particular, $L_{am}$ exhibited an interesting behaviour. As reported in the literature, the absorbed water acts as a plasticizer and progressively reduces the glass transition temperature ($T_g$) of amorphous lactose (Buckton and Darcy, 1995; Sheokand et al., 2014). After the $T_g$ falls below the temperature of the experiment, molecular mobility is suddenly increased, the amorphous lactose recrystallizes and the absorbed water is expelled causing a subsequent loss of weight (Buckton, 1997). For the tested amorphous lactose, this event occurred at 60 % RH. During the crystallization both

α- and β-lactose might be generated in different ratios (Timmermann et al., 2006; Vollenbroek et al., 2010). The resulting crystalline form showed significant water sorption only at high level of relative humidity (RH ≥ 90%). Interestingly, at 60% RH the two stable crystalline lactose forms (L$\alpha \cdot H_2O$ and $L\alpha_S$) presented a steady profile, while the metastable crystalline $L\alpha_H$ showed very limited weight increment.

On the other hand, at 80% RH $L\alpha_H$ was the only form presenting a significant weight increase (0.5%), while all the others afforded an almost insignificant weight gain (< 0.1%).

Finally, at 85% RH $L\alpha_S$ showed a sharp weight increase (5.2%), whereas, among the other forms, only $L\alpha_H$ presented a limited weigh gain (0.5%). The differences in the amount of water absorbed by each form of lactose at the three specific RH values were exploited for quantitation purpose.

To assess the existence of a correlation between the weight change of a sample at a certain value of relative humidity and the amount of a specific form of lactose present in the sample, three different sets of binary physical mixtures were prepared. The mixtures of the first set were composed of L$\alpha \cdot H_2O$ and different percentages (5, 10, 20, 50, 100% w/w) of $L_{am}$. In the second and the third set $L_{am}$ was replaced by either $L\alpha_H$ or $L\alpha_S$ respectively. For each value of relative humidity (60%, 80% and 85%) the contributions of $L_{am}$ ($y_{RH}^{am}$), $L\alpha_H$ ($y_{RH}^{H}$) and $L\alpha_S$ ($y_{RH}^{S}$) to the total weight variation ($y_{RH}$) were evaluated. The data obtained by plotting the weight variation as a function of the amount of each lactose form in the binary mixtures were submitted to linear regression under the following assumption: when the intercept was statistically different from the blank (pure L$\alpha \cdot H_2O$) it was taken as such, otherwise the value relevant to the blank was used as intercept of the straight line equation in the following steps of data elaboration.

Figure 22 (left) reports the effect of the presence of $L_{am}$ in the binary mixtures on the weight variation at 60% RH. The existence of a good linear correlation between the amount of $L_{am}$ and the weight loss ($y_{60}^{am} = -0.0995 \cdot L_{am} + 0.2431$; $R^2 = 0.9977$) was highlighted. On the contrary, increasing amounts of $L\alpha_H$ afforded an increasing weight gain, although in this case the effect was less evident ($y_{60}^{H} = 0.0015 \cdot L\alpha_H - 0.0144$; $R^2 = 0.9628$) (Figure 22, right). Different amounts of $L\alpha_S$ caused a constant and statistically not significant response ($y_{60}^{S} = -0.0943$[7]).

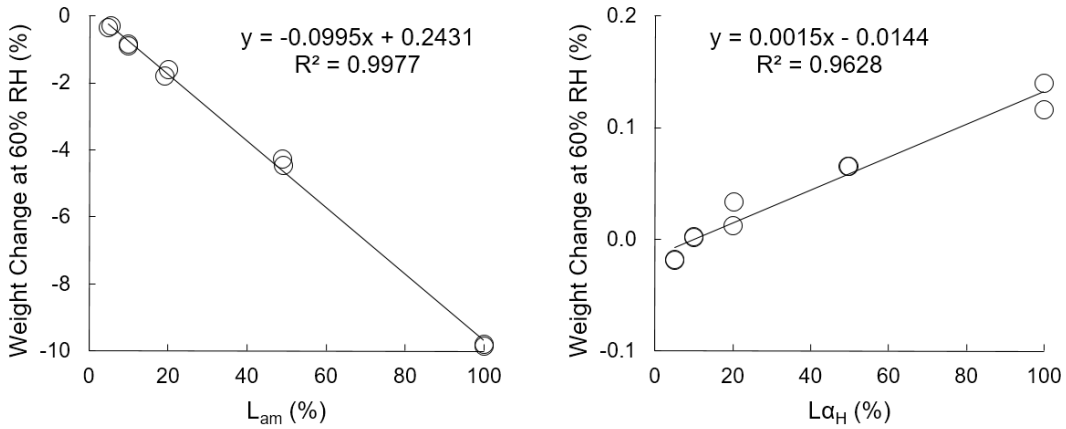


**Figure 22** Weight change at 60% RH *vs* $L_{am}$ content in binary mixtures of $L_{am}$ and $L\alpha{\cdot}H_2O$ (left). Weight change at 60% RH *vs* $L\alpha_H$ content in binary mixtures of $L\alpha_H$ and $L\alpha{\cdot}H_2O$ (right).

Thus, the overall weight change at 60% RH could be expressed as the sum of three contributions:

$$y_{60} \cong y_{60}^{am} + y_{60}^{H} + y_{60}^{S} \cong -0.0995 \cdot L_{am} + 0.0015 \cdot L\alpha_H + 0.0762 \qquad [3]$$

where the constant term was assumed, as a first approximation, as the average of the constant terms in $y_{60}^{am}$, $y_{60}^{H}$ and $y_{60}^{S}$. This assumption was made by considering that the

[7] Difference from blank value (0 at 60% RH) statistically not significant.

intercepts of the regression lines and the constant term have the same physical meaning, namely the response of the blank (pure $L\alpha \cdot H_2O$).

As previously reported, the reference sample of $L_{am}$ consisted of 46% β-form. In order to evaluate the effect of $L_{am}$ anomeric composition on vapour sorption, three additional samples of amorphous lactose with different α/β ratio were prepared. The anomeric composition of each sample was determined once again by $^1$H NMR (see section 3.2.5). The obtained results are shown in Figure 23.

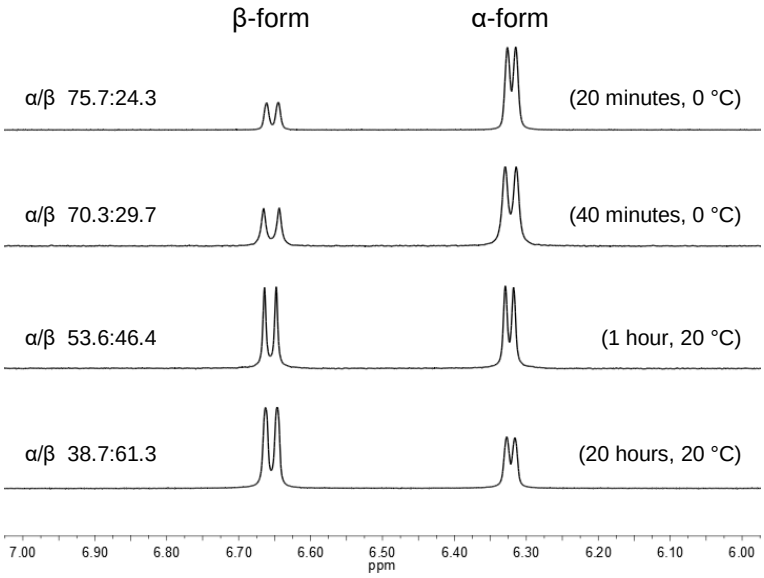


**Figure 23** $^1$H NMR spectra in the 6-7 ppm region and relevant anomeric compositions of the produced $L_{am}$ samples. For each sample, the time and the temperature at which the feed solution was kept under stirring before being spray dried are reported in brackets.

Pure amorphous lactose samples were subject to vapour sorption isotherms in the 5-90% RH range and gave profiles similar to the one previously obtained for $L_{am}$, which differed from each other for the extent of the weight loss at 60% RH. A relationship between such loss of weight and the percentage of α-form in each amorphous sample was sought and a quite good linear correlation was found (Figure 24).

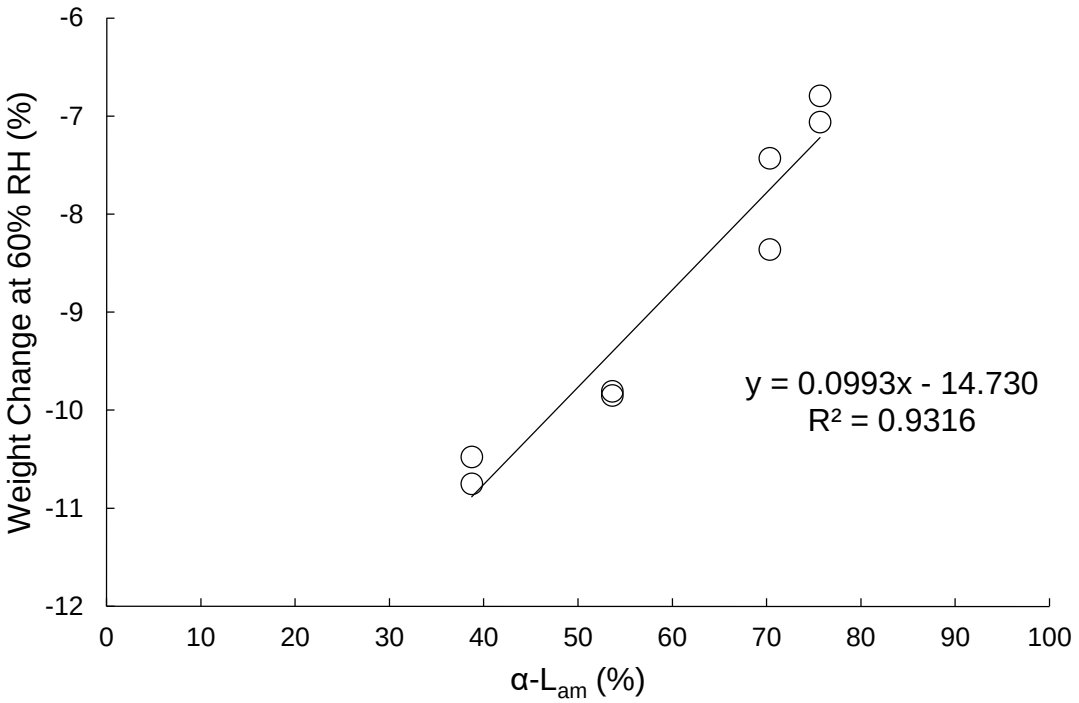


**Figure 24** Weight change at 60% RH *vs* α-form percentage in pure amorphous lactose samples.

Thus, the weight loss theoretically produced by a pure amorphous sample consisting of 100% α-form was calculated by extrapolation. The ratio between this weight loss (-4.8%) and that produced by $L_{am}$ containing 46% β-form (-9.4%) provided a correction coefficient that was eventually applied (by multiplying) to $y_{60}^{am}$, namely the contribution of $L_{am}$ to the weight variation at 60% RH.

Equation 3 was then updated introducing the corrected $y_{60}^{am}$ and a new equation describing the overall weight variation of pure α-lactose samples at 60% RH was obtained:

$$y_{60} \cong -0.0508 \cdot L_{am} + 0.0015 \cdot L\alpha_H + 0.0366 \qquad [4]$$

At 80% RH the major contribution to the weight gain was given by the presence of $L\alpha_H$

($y_{80}^{H} = 0.0052 \cdot L\alpha_H + 0.0108$[8]; $R^2 = 0.9990$) (Figure 25, left). A linear correlation was found also between the amount of $L\alpha_S$ and the extent of the weight gain ($y_{80}^{S} = 0.0008 \cdot L\alpha_S + 0.0199$[8]; $R^2 = 0.9900$) (Figure 25, right). $L_{am}$ was responsible for a minimal weight gain regardless of the percentage in which it was present in the mixture ($y_{80}^{am} = 0.0147$[8]).

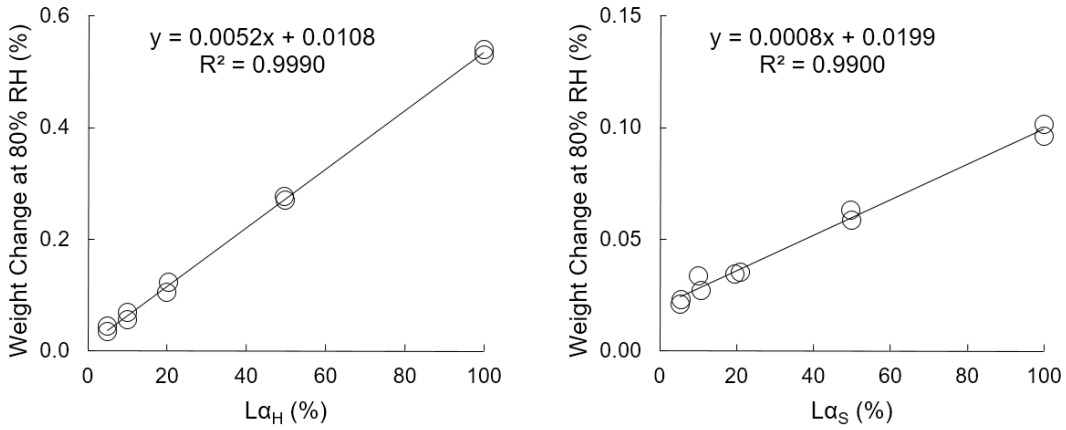


**Figure 25** Weight change at 80% RH *vs* $L\alpha_H$ content in binary mixtures of $L\alpha_H$ and $L\alpha{\cdot}H_2O$ (left). Weight change at 80% RH *vs* $L\alpha_S$ content in binary mixtures of $L\alpha_S$ and $L\alpha{\cdot}H_2O$ (right).

The total weight change at 80% RH was expressed as:

$$y_{80} \cong y_{80}^{H} + y_{80}^{S} + y_{80}^{am} \cong 0.0052 \cdot L\alpha_H + 0.0008 \cdot L\alpha_S + 0.0198 \qquad [5]$$

where the constant term was calculated in the same manner as for Equation 3, as the average of the constant terms in $y_{80}^{H}$, $y_{80}^{S}$ and $y_{80}^{am}$.

Finally, at 85% RH the weight gain was proportional to the quantity of both $L\alpha_S$ and $L\alpha_H$. The effect was much stronger in the case of $L\alpha_S$ ($y_{85}^{S} = 0.0533 \cdot L\alpha_S - 0.1115$; $R^2 = 0.9988$) (Figure 26, left) than for $L\alpha_H$ ($y_{85}^{H} = 0.0052 \cdot L\alpha_H + 0.0497$; $R^2 = 0.9667$)

[8] Difference from blank value (0.0198 at 80% RH) statistically not significant.

(Figure 26, right). The presence of $L_{am}$ did not significantly affect the weight change of the sample and a constant response was observed ($y_{85}^{am} = 0.0468$[9]).

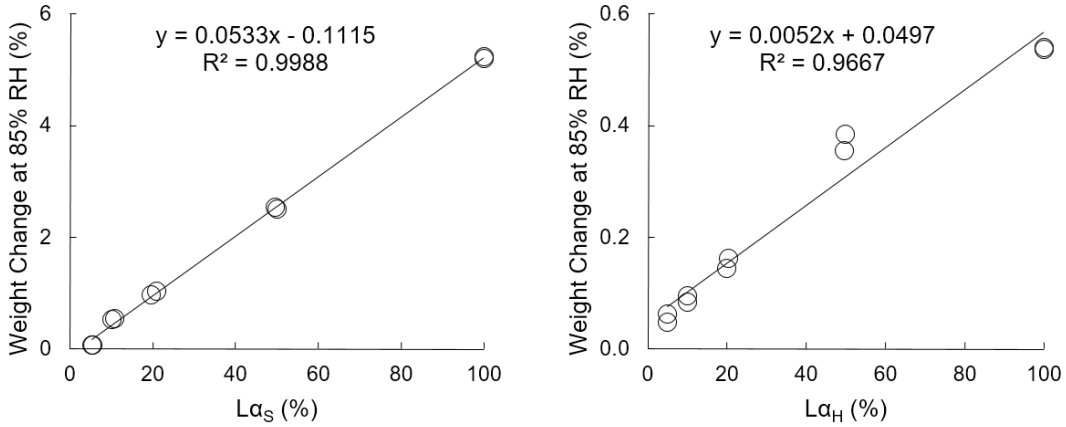


**Figure 26** Weight change at 85% RH *vs* $L\alpha_S$ content in binary mixtures of $L\alpha_S$ and $L\alpha{\cdot}H_2O$ (left). Weight change at 85% RH *vs* $L\alpha_H$ content in binary mixtures of $L\alpha_H$ and $L\alpha{\cdot}H_2O$ (right).

Once again the total weight change at 85% RH was calculated as:

$$y_{85} \cong y_{85}^{S} + y_{85}^{H} + y_{85}^{am} \cong 0.0533 \cdot L\alpha_S + 0.0052 \cdot L\alpha_H - 0.0097 \qquad [6]$$

also in this case, the constant term was obtained as the arithmetical mean of the constant terms in $y_{85}^{S}$, $y_{85}^{H}$ and $y_{85}^{am}$.

Equations 5 and 6 were combined in a system of two equations in two variables to compute the values of $L\alpha_S$ and $L\alpha_H$. Then, $L\alpha_H$ was substituted in Equation 4 to get $L_{am}$. The percentages of each form of lactose in a given sample were, therefore, calculated as:

$$L_{am} = -19.6882 \cdot y_{60} + 5.5938 \cdot y_{80} - 0.0834 \cdot y_{85} + 0.6085 \qquad [7]$$

$$L\alpha_H = 193.7335 \cdot y_{80} - 2.8871 \cdot y_{85} - 3.8647 \qquad [8]$$

$$L\alpha_S = -18.8122 \cdot y_{80} + 19.0333 \cdot y_{85} + 0.5564 \qquad [9]$$

[9] Difference from blank value (0.0329 at 85% RH) statistically not significant.

In order to check the effective applicability of the method, four physical mixtures containing different amounts of $L\alpha \cdot H_2O$, $L\alpha_H$ and $L_{am}$ were prepared. Since the amorphous lactose used for the preparation of these test mixtures was $L_{am}$ containing a known amount of β-form (i.e., 46%), in this case the correction for pure α-lactose samples was not applied. Table 4 shows the actual and the calculated percentages of $L\alpha_H$ and $L_{am}$ in the mixtures.

**Table 4** Actual and calculated percentages (w/w) of $L\alpha_H$ and $L_{am}$ in the test mixtures.

| Mixture | $L\alpha_H$ (%) | | $L_{am}$ (%) | |
|---|---|---|---|---|
| | Actual | Calculated | Actual | Calculated |
| 1 | 7.3 | 8.4 | 5.4 | 4.9 |
| 2 | 9.8 | 8.2 | 11.8 | 10.0 |
| 3 | 13.7 | 13.1 | 9.4 | 8.5 |
| 4 | 19.9 | 17.3 | 18.9 | 17.7 |

The amounts of $L\alpha_H$ and $L_{am}$ calculated according to the proposed method showed an acceptable accuracy with good adherence to reality; the error relevant to each component was always below 2.6% with respect to the overall composition of the mixture. This can be considered satisfactory for practical use, especially taking into account that the amounts of the two lactose forms in the mixtures were relatively low.

These results strongly suggest that the method can be used for the identification and quantification of the forms of lactose that might be generated as a consequence of the micronization process even when they are simultaneously present in the same sample.

Therefore, the method was used to quantitatively determine the composition of a micronized lactose sample produced on an industrial scale apparatus (Lacto-Sphere® MM3). According to the producer, this micronized lactose was obtained starting from the

same coarse α-lactose monohydrate used in the present research project, but using air instead of nitrogen as fluid for the micronization.

The analysis could not be performed on Lactose-7 and Lactose-2 because the above-mentioned conversion of the metastable anhydrous α-lactose into α-lactose monohydrate occurred in a relatively short time after DSC measurements; thus, at the time the method was completed, all the metastable phase had already reconverted into the stable one.

Lacto-Sphere® MM3 was characterized by a degree of crystallinity, $C$, of 58 ± 1 (see section 3.2.6) and its DSC trace (Figure 27, left) was similar to that of Lactose-7 (Figure 19, curve f). Therefore, it was assumed that this lactose powder contained a certain amount of $L\alpha_H$ with no or very little amount of $L_{am}$.

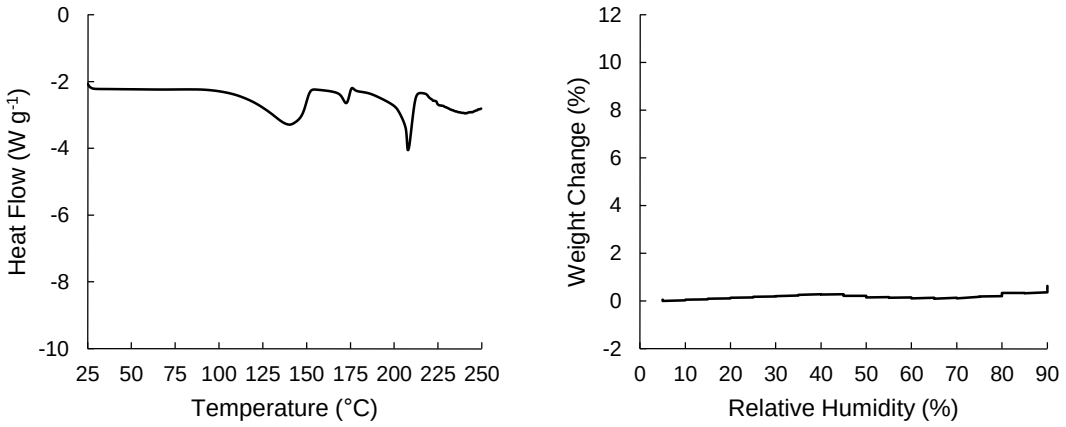


**Figure 27** DSC trace (left) and DVS profile (right) of Lacto-Sphere® MM3.

$^1$H NMR analysis of Lacto-Sphere® MM3 revealed the presence of a negligible amount of β-form (1.5 ± 0.2%). Once again this datum indicates that micronization did not induce mutarotation (t-test, $p > 0.05$). Thus, the DVS method developed for pure α-lactose samples could be applied. After recording the DVS profile (Figure 27, right), data processing according to Equations 7-9 afforded the following composition: 74.8% α-lactose monohydrate, 23.0% hygroscopic anhydrous α-lactose and 2.2% amorphous

lactose; stable anhydrous α-lactose was not detected. This outcome was in agreement with the results obtained by DSC and confirmed that hygroscopic anhydrous α-lactose was generated in relatively large amount in the micronization process, with a very low or negligible fraction of amorphous material.

## 4.3. Effect of Lactose Solid-State on Drug Respirability

### 4.3.1. Ternary Mixtures

Lactose-2 was chosen to be used as fine component in the preparation of ternary mixtures including Lacto-Sphere® MM50 (Lα·$H_2O$) as carrier and 1% w/w salbutamol sulphate (SS). Three mixtures containing variable amounts of fine micronized lactose were prepared according to the compositions reported in Table 5. A binary mixture including no fines (mixture M-SS) was prepared as reference.

**Table 5** Composition (% w/w) of the studied ternary mixtures.

| Mixture | Lα·$H_2O$ (%) | Lactose-2 (%) | SS (%) |
|---|---|---|---|
| M-SS | 99 | - | 1 |
| M-10 | 89 | 10 | 1 |
| M-30 | 69 | 30 | 1 |
| M-50 | 49 | 50 | 1 |

As the percentage of lactose fines in the mixtures increased, a reduced homogeneity was observed. While the calculated coefficient of variation (see section 3.2.14) remained below 5% for the first three mixtures, in the case of mixture M-50 an additional mixing step of 120 minutes was necessary to achieve the fixed level of homogeneity.

Table 6 reports the emitted dose (ED), fine particle dose (FPD) and fine particle fraction (FPF) obtained for each mixture.

The positive effect of lactose fines on the aerosolization performance was confirmed. In particular, best results were achieved with the mixture containing 30% of Lactose-2 (mixture M-30). The FPD obtained in this case was almost four times greater than that provided by mixture M-SS (containing no added fines). On the other hand, the presence

of a substantial amount of Lactose-2 in mixture M-50 led to a significant decrease of the ED, due to the formation of agglomerates which remained in the capsules during the aerosolization.

**Table 6** ED, FPD and FPF of salbutamol sulphate from the tested mixtures.

| Mixture | ED (µg) | FPD (µg) | FPF (%) |
|---|---|---|---|
| M-SS | 177.1 ± 3.4 | 26.8 ± 1.9 | 15.1 ± 0.8 |
| M-10 | 178.7 ± 4.6 | 84.3 ± 2.6 | 47.2 ± 0.7 |
| M-30 | 180.9 ± 9.7 | 103.4 ± 7.3 | 57.2 ± 2.5 |
| M-50 | 102.8 ± 5.5 | 34.9 ± 4.6 | 33.9 ± 2.8 |

The ternary mixtures were then stored under two different conditions of temperature and relative humidity: 25 °C, 60% RH and 40 °C, 75% RH. *In vitro* aerodynamic assessment was repeated after 2, 3 and 6 months for the first storage condition and after 2 and 3 months for the second one. Powders were stored in these conditions in glass vials stoppered with high-density PET caps. Figure 28 shows the trend of the FPDs produced by the aged mixtures.

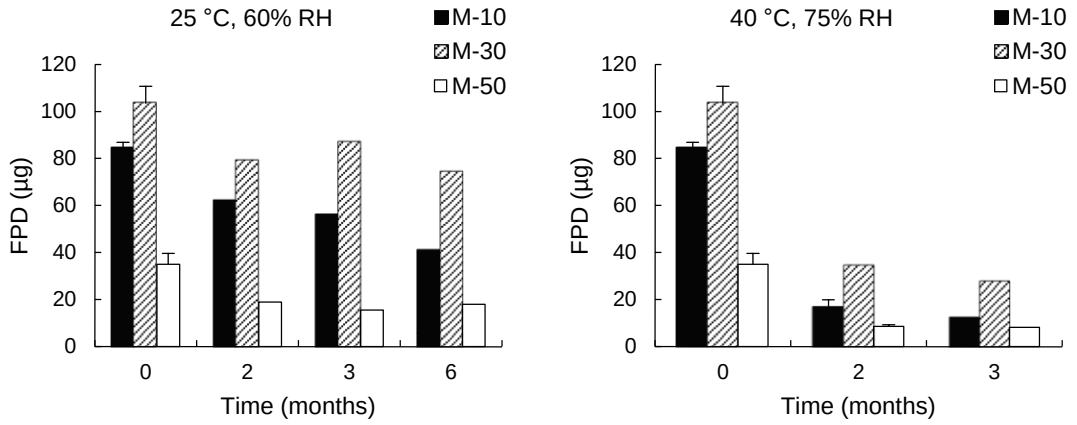


**Figure 28** FPD of salbutamol sulphate from ternary mixtures stored at 25 °C, 60% RH (left) and 40 °C, 75% RH (right).

Stability testing revealed a progressive worsening of the aerosolization performance with aging, especially when mixtures were stored at 40 °C, 75% RH. The absorption of moisture may have led to increased capillary forces between the adhering particles within the mixtures, thus resulting in a more difficult detachment of the drug during aerosolization (Guenette et al., 2009). The development of unfavourable interactions between lactose and drug could be due also to the fact that Lactose-2 contained unstable components (i.e., hygroscopic anhydrous α-lactose and amorphous lactose) which continuously evolved over time. In this regard, Figure 29 shows the evolution of the DSC trace of Lactose-2 during aging. DSC measurements were performed alongside the *in vitro* aerodynamic assessment on samples of Lactose-2 stored at 25 °C, 60% RH.

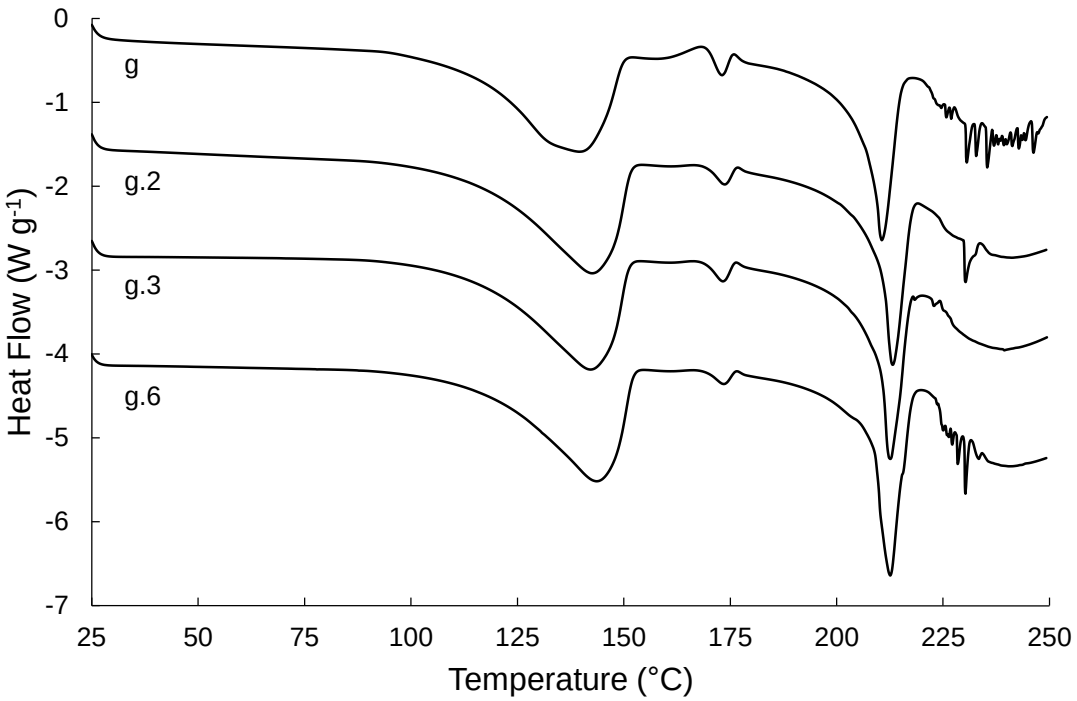


**Figure 29** DSC traces of Lactose-2 recorded immediately after production (g) and after 2 (g.2), 3 (g.3) and 6 (g.6) months storage at 25 °C, 60% RH.

The thermal events in the region between the evaporation of crystalline water and the melting of lactose progressively decreased in intensity during aging. This was indicative

of the partial conversion of hygroscopic anhydrous α-lactose and amorphous lactose mainly into α-lactose monohydrate (although the possible formation of small amounts of mixed α/β compounds could not be excluded a priori). Such transformations would be obviously favoured under higher RH conditions.

These results suggested that a strong relationship between the nature of the solid-state of micronized lactose and the aerosolization performance may exist. Thus, differently from what is commonly reported in the literature, the positive effect of lactose fines would depend not only on their reduced size, but also on a specific characteristic of their solid-state leading to a decrease of the surface interaction with the drug.

In order to test this hypothesis, different lactose polymorphs were selected to be employed as carriers in the preparation of binary mixtures.

### 4.3.2. Binary Mixtures

Taking into consideration the results reported in sections 4.1 and 4.2, it was assumed that $L\alpha_H$ is presumably the major component of the surface of micronized lactose particles; thus, it was chosen as one of the alternative carriers to be tested. $L\alpha_S$ was selected because of its anhydrous character associated with a higher stability.

It is worth recalling here that both the anhydrous α-lactose polymorphs were prepared starting from $L\alpha{\cdot}H_2O$. Therefore, they were evaluated in terms of dimensional distribution and compared to $L\alpha{\cdot}H_2O$, which was previously used as carrier. The obtained results are reported in Table 7.

**Table 7** Particle size distribution parameters of the lactose samples used as carriers in binary mixtures.

| Sample | $d_{V10}$ (µm) | $d_{V50}$ (µm) | $d_{V90}$ (µm) |
|---|---|---|---|
| Lα·$H_2O$ | 10.2 ± 0.8 | 53.1 ± 2.0 | 103.3 ± 2.6 |
| $L\alpha_S$ | 20.7 ± 2.2 | 56.3 ± 0.4 | 105.7 ± 1.4 |
| $L\alpha_H$ | 18.8 ± 1.1 | 54.7 ± 0.8 | 104.9 ± 0.6 |

The carriers exhibited similar $d_{V50}$ and $d_{V90}$, but different $d_{V10}$, with the anhydrous forms containing lower amounts of intrinsic fines, which probably coalesced during thermal dehydration. As previously reported, reduced percentages of fines could detrimentally affect the aerosolization performance of the corresponding mixtures.

Morphology and surface characteristics of the carriers were visually evaluated by scanning electron microscopy (SEM). Figures 30-32 show the SEM micrographs collected for Lα·$H_2O$, $L\alpha_S$ and $L\alpha_H$, respectively.

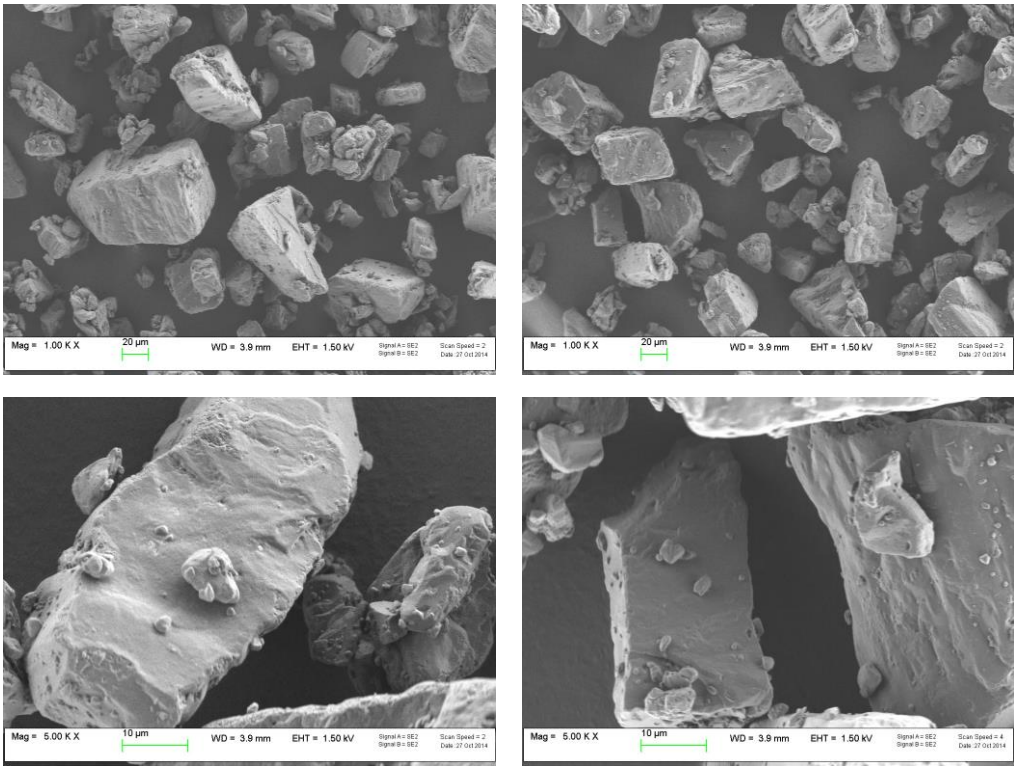


**Figure 30** SEM images of Lα·$H_2O$ (1000x and 5000x magnifications).

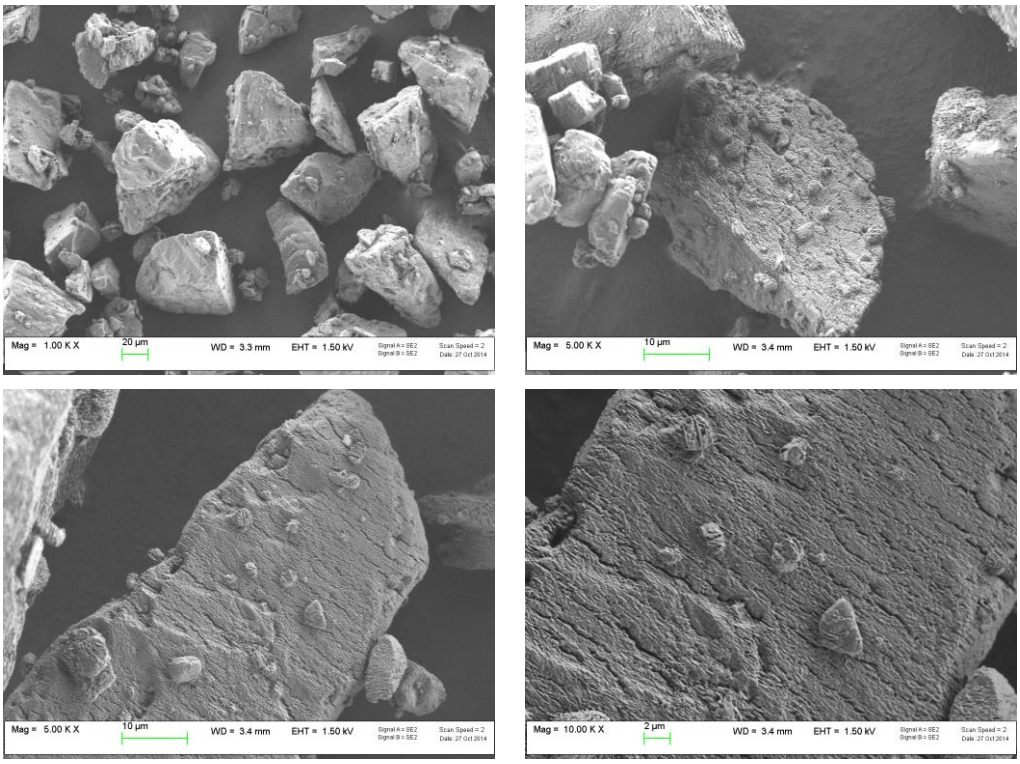


**Figure 31** SEM images of $L\alpha_S$ (1000x, 5000x and 10000x magnifications).

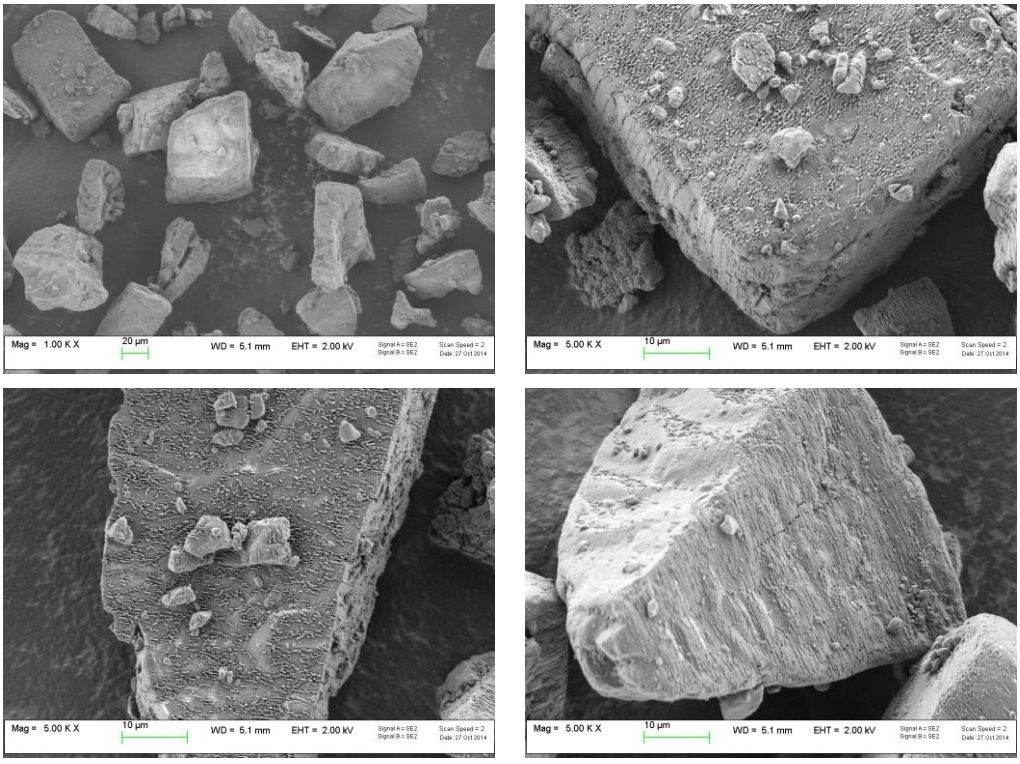


**Figure 32** SEM images of $L\alpha_H$ (1000x and 5000x magnifications).

The three samples of lactose were composed of particles with similar size and shape, but different surface characteristics. In particular, the surface of L$\alpha$·$H_2O$ particles was irregular, but smoother than that of the other polymorphs. Roughness progressively increased in L$\alpha_H$ and L$\alpha_S$ particles, which showed more clefts and defects, likely ascribable to the higher temperature used during the preparation of the stable polymorph.

Then, L$\alpha_S$ and L$\alpha_H$ were used to prepare two binary mixtures, S-SS and H-SS, containing 1% w/w salbutamol sulphate. These mixtures were tested through *in vitro* aerodynamic assessment and compared to the binary mixture employing L$\alpha$·$H_2O$ as carrier (mixture M-SS). The obtained results are reported in Table 8.

**Table 8** ED, FPD and FPF of salbutamol sulphate from the tested binary mixtures.

| Mixture | ED (µg) | FPD (µg) | FPF (%) |
|---|---|---|---|
| M-SS | 177.1 ± 3.4 | 26.8 ± 1.9 | 15.1 ± 0.8 |
| S-SS | 173.0 ± 2.7 | 54.4 ± 2.2 | 31.5 ± 0.9 |
| H-SS | 182.7 ± 11.6 | 76.2 ± 3.6 | 41.7 ± 1.9 |

The use, as carriers, of anhydrous α-lactose forms was found to have a remarkable positive effect on the deposition of salbutamol sulphate, thus confirming the key role of lactose solid-state in affecting the aerosolization performance. In both cases, the produced FPF was significantly higher than that obtained with L$\alpha$·$H_2O$. In particular, the mixture with L$\alpha_H$ gave ED, FPD and FPF close to those provided by the ternary mixture containing 10% of fines (mixture M-10) (Figure 33).

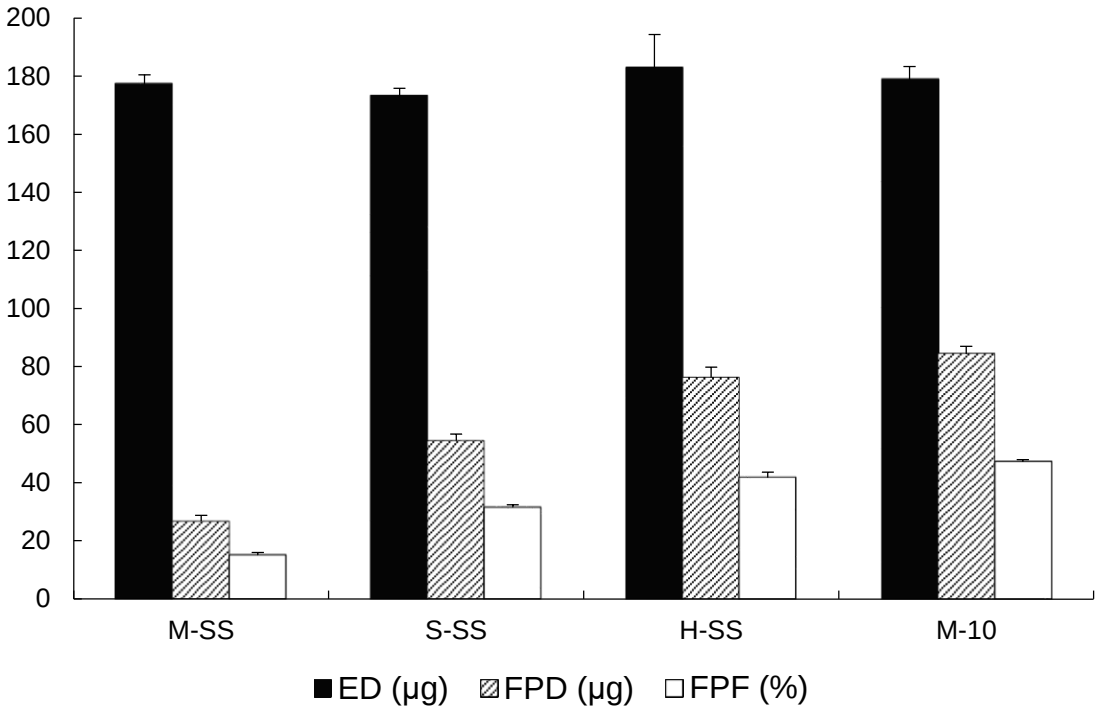


**Figure 33** ED, FPD and FPF of salbutamol sulphate obtained from binary mixtures and mixture M-10.

Moreover, it is worth to underline that the use of anhydrous α-lactose polymorphs provided better results with respect to the hydrate form, despite they contained a significantly lower amount of fines.

In order to evaluate the influence of lactose solid-state on the respirability of a drug with more lipophilic characteristics, budesonide (BUD) was chosen as alternative model API. $L\alpha \cdot H_2O$ and $L\alpha_S$ were then used for the preparation of two binary mixtures, M-BUD and S-BUD, containing 1% w/w budesonide.

Table 9 shows the results of the *in vitro* aerodynamic assessment performed on the prepared mixtures.

**Table 9** ED, FPD and FPF of budesonide from the tested binary mixtures.

| Mixture | ED (µg) | FPD (µg) | FPF (%) |
|---|---|---|---|
| M-BUD | 154.1 ± 4.3 | 27.9 ± 0.1 | 18.1 ± 0.5 |
| S-BUD | 149.6 ± 4.0 | 17.9 ± 1.3 | 12.0 ± 0.5 |

In this case, the use of an anhydrous carrier ($L\alpha_S$) negatively affected the performance of aerosolization resulting in a decrease of the FPF. Though in an opposite way to what was observed with salbutamol sulphate, even in this case the nature of lactose solid-state played an important role in determining the interaction between carrier and drug and the final deposition of the latter.

## 4.4. Characterization of Surface Energy by IGC

Data presented in section 4.3 clearly underline the role of the solid-state properties of the carrier on the aerosolization performance of APIs with different physico-chemical characteristics, thus putting into evidence the relevance of the thermodynamic state of the carrier surface. In order to shed light on this aspect, inverse gas chromatography (IGC) was selected as a tool to investigate possible energy variations among the lactose carriers and the APIs under investigation.

This part of the research project was carried out during a six-month scholarship at the Purdue University in West Lafayette (Indiana, USA) under the supervision of Prof. Teresa Carvajal (Department of Agricultural and Biological Engineering, ABE) and Prof. Rodolfo Pinal (Department of Industrial and Physical Pharmacy, IPPH).

### 4.4.1. IGC Theory

Inverse gas chromatography is a technique commonly used to study the surface energetics of powder samples. It has several advantages such as the ability to analyse samples without pre-treatment, avoiding any manipulation that may alter the nature of the surface being studied, the possibility to perform experiments under a wide range of controlled conditions in terms of temperature and relative humidity and a high level of reproducibility. Moreover, differently from techniques such as AFM, IGC probes the surface properties of an entire sample of material. On the other hand, a factor to be considered is the long time needed for analysis (Grimsey et al., 2002).

In summary, an inert gas carrier is flowed at a constant rate through a column packed with the sample under investigation (which represents the stationary phase). Vapours of

organic probes are individually injected into the system and give different retention times depending on their interaction with the surface of the sample. The retention time is converted into the retention volume $V_N$, namely the volume of carrier gas required to elute a probe, that is given by:

$$V_N = jF(t_R - t_0) \quad [10]$$

where $j$ is a correction factor taking into account the pressure drop across the packed column, $F$ is the carrier gas flow rate, $t_R$ is the retention time of the probe and $t_0$ is the void retention time (i.e., the time required to elute an inert elutant). The standard free energy of adsorption, $\Delta G_A$, of the probe on the sample can be then calculated as:

$$-\Delta G_A = RTlnV_N + K_1 \quad [11]$$

where $R$ is the gas constant, $T$ is the column temperature and $K_1$ is a constant term encompassing the choice of the standard state for $\Delta G_A$ and the surface area of the sample (Tong et al., 2002). $\Delta G_A$ represents the starting point to determine the surface (free) energy, $\gamma_S$, of a sample.

Surface free energy can be divided into a dispersive ($\gamma_S^D$) and specific ($\gamma_S^{SP}$) component:

$$\gamma_S = \gamma_S^D + \gamma_S^{SP} \quad [12]$$

While the dispersive contribution relates to non-specific van der Waals forces, the specific contribution is related to other kinds of interactions, such as hydrogen bonding and acid-base forces (Jones et al., 2012).

Dispersive surface energy is determined by injecting a series of non-polar probes (*n*-alkanes) at infinite dilution, so as to avoid interactions between probe molecules or

competition for the binding sites (Buckton and Gill, 2007). Having no dipole moment nor functional groups which undergo specific interactions, *n*-alkanes can only interact by induced dipole forces. Dispersive surface energy is usually obtained from an equation representing the relationship between the free energy of adsorption and the work of adhesion in the case of purely dispersive forces:

$$RTlnV_N = 2N(\gamma_S^D)^{1/2} a(\gamma_L^D)^{1/2} + K_2 \qquad [13]$$

where $N$ is Avogadro's number, $a$ the surface area of the probe, $\gamma_L^D$ the dispersive surface tension of the probe and $K_2$ a constant encompassing the choice of the standard state for $\Delta G_A$ and the surface area of the sample.

Thus, $\gamma_S^D$ can be determined from the slope of the straight line obtained by plotting $RTlnV_N$ against $a(\gamma_L^D)^{1/2}$ (Schultz et al., 1987) (Figure 34).

To determine the specific surface energy, various polar probes are injected. These probes interact with the sample via both dispersive and specific interactions. The specific component of free energy of adsorption, $\Delta G_A^{SP}$, is calculated by subtracting the dispersive contribution from the total free energy of adsorption. This is obtained by measuring the vertical distance between the polar probe datum and the alkane reference line in the previously mentioned plot (Figure 34). Then, two different approaches can be followed.

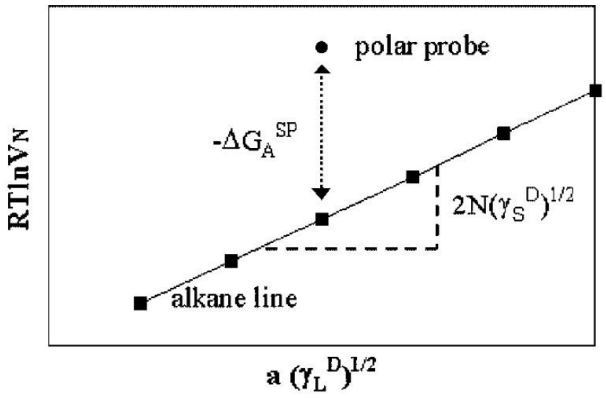


**Figure 34** Method to determine the dispersive surface energy ($\gamma_S^D$) and the specific component of the free energy of adsorption ($\Delta G_A^{SP}$) (Grimsey et al., 2002, reprinted with permission).

The first approach was introduced by Schultz et al. (Schultz et al., 1987) and results in the calculation of an acidic or electron accepting parameter ($K_A$) and a basic or electron donating parameter ($K_D$) describing the acid and base characteristics of the material under investigation. These parameters are derived from $\Delta G_A^{SP}$ through the following equation:

$$-\Delta G_A^{SP}/AN^* = K_A(DN/AN^*) + K_D \quad [14]$$

where $DN$ is the electron donor or base number (Gutmann, 1978) and $AN^*$ is the corrected electron acceptor or acid number (Riddle and Fowkes, 1990), which define the basicity and the acidity of the probe, respectively. By plotting $-\Delta G_A^{SP}/AN^*$ against $DN/AN^*$ a straight line is obtained. $K_A$ and $K_D$ correspond to the slope and the intercept of the line, respectively (Tong et al., 2002). The major disadvantage of this approach is that $K_A$ and $K_D$ are dimensionless numbers and cannot be used in further meaningful calculations.

A second method proposed by van Oss (van Oss, 2006) divides the specific surface energy into an acid (Lewis acceptor) contribution ($\gamma_S^+$) and a base (Lewis donor) contribution ($\gamma_S^-$), which can be calculated from:

$$-\Delta G_A^{SP} = 2aN((\gamma_L^- \cdot \gamma_S^+)^{1/2} + (\gamma_L^+ \cdot \gamma_S^-)^{1/2}) \quad [15]$$

where $\gamma_L^-$ and $\gamma_L^+$ are the electron donor and the electron acceptor parameter of the surface tension of the probe, respectively. Thus, the injection of two monopolar probes with opposite polarities (e.g., ethyl acetate and chloroform) allows to determine $\gamma_S^+$ and $\gamma_S^-$, which are eventually combined to calculate the specific surface energy, $\gamma_S^{SP}$, as:

$$\gamma_S^{SP} = 2(\gamma_S^+ \cdot \gamma_S^-)^{1/2} \quad [16]$$

The total surface energy is then obtained from the sum of the dispersive and specific components (as shown in Equation 12).

### 4.4.2. Dispersive Surface Energy

Dispersive surface energy was determined for lactose carriers (Lα·$H_2O$, $L\alpha_S$ and $L\alpha_H$) and the selected APIs (SS and BUD). Measurements were carried out at two different levels of relative humidity: 0% RH, in order to analyse the samples under inert conditions, preventing water sorption by $L\alpha_H$ and its possible conversion into Lα·$H_2O$, and 60% RH, with the aim to mimic the ambient conditions likely occurring within a DPI. The obtained results are reported in Table 10.

**Table 10** Dispersive surface energy, $\gamma_S^D$, of the samples analysed at 0% RH and 60% RH.

| Sample | $\gamma_S^D$ at 0% RH (mJ $m^{-2}$) | $\gamma_S^D$ at 60% RH (mJ $m^{-2}$) |
|---|---|---|
| Lα·$H_2O$ | 35.5 ± 1.3 | 27.8 ± 1.1 |
| $L\alpha_S$ | 42.1 ± 1.4 | 35.4 ± 0.8 |
| $L\alpha_H$ | 48.5 ± 1.5 | 36.3 ± 0.2 |
| SS | 52.5 ± 0.5 | 45.5 ± 0.5 |
| BUD | 46.2 ± 0.2 | 44.5 ± 0.5 |

$\gamma_S^D$ values obtained at both levels of relative humidity exhibited similar trends. In particular, the dispersive surface energy of lactose carriers progressively increased following the order Lα·$H_2O$ < $L\alpha_S$ < $L\alpha_H$ at 0% RH and Lα·$H_2O$ < $L\alpha_S$ ≈ $L\alpha_H$ (t-test, $p > 0.05$) at 60% RH. This tendency may be explained by the more defective surface of the anhydrous polymorphs of α-lactose (see Figure 31 and Figure 32), which is a direct consequence of the dehydration process through which they were prepared.

In general, measurements performed at 60% RH produced lower values of $\gamma_S^D$, presumably due to the adsorption of water molecules, which hindered the surface of the samples and led to a reduction of the interactions with the *n*-alkanes used as probes. While this was particularly true in the case of $L\alpha_H$, the dispersive surface energy of budesonide remained almost unchanged, in agreement with its lipophilic nature.

### 4.4.3. Specific Surface Energy

The specific free energy of adsorption, $\Delta G_A^{SP}$, of a series of polar probes was determined at 60% RH. Figure 35 reports the results obtained for the analysed samples.

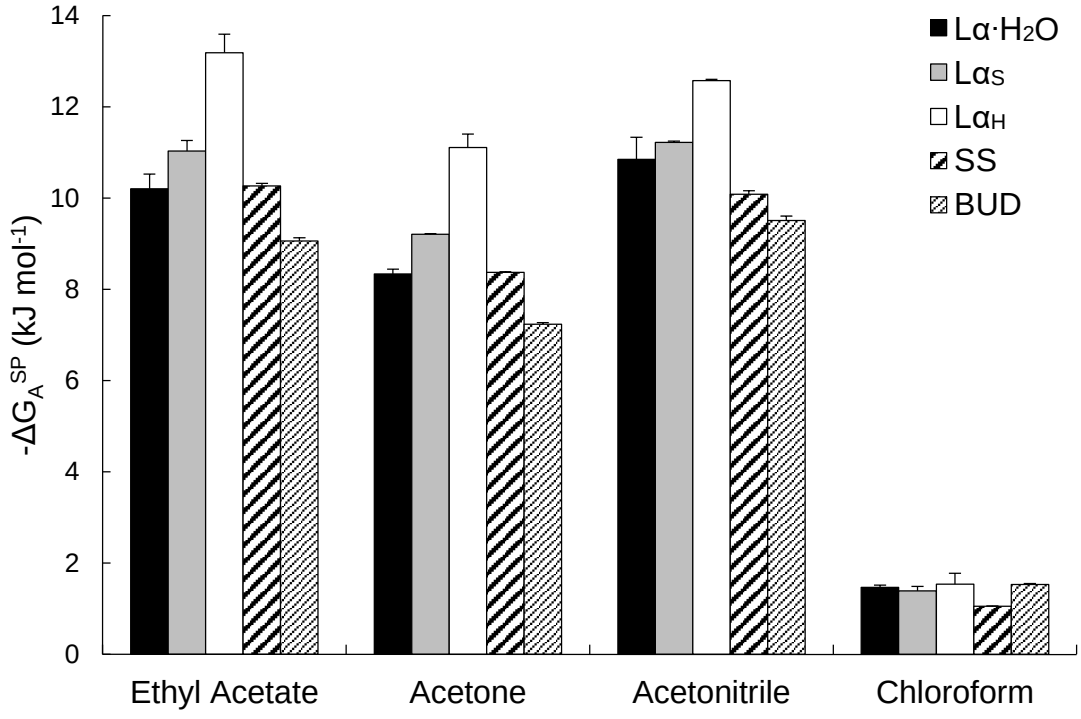


**Figure 35** Specific free energy of adsorption, $\Delta G_A^{SP}$, of lactose carriers and APIs determined at 60% RH.

While the order of magnitude of the interaction with the different probes was defined by the intrinsic characteristics of each selected probe, the trend of the interactions given by the analysed samples with a specific probe was taken into account to evaluate the

propensity of each sample to behave as electron donor/acceptor. Thus, the data reported in this section have been considered for their relative positioning, rather than for their absolute value. Lactose carriers exhibited increasing polar interactions with the basic (ethyl acetate) and the amphoteric (acetone and acetonitrile) probes in the order $L\alpha \cdot H_2O$ < $L\alpha_S$ < $L\alpha_H$. Differently, interactions with the acidic chloroform were comparable (ANOVA, $p > 0.05$). As regards the APIs, basic and amphoteric probes gave stronger interactions with salbutamol sulphate than with budesonide. Accordingly, chloroform was more reactive towards budesonide.

Starting from these data, both Schultz and van Oss approaches were adopted. Unfortunately, the application of the first method did not result in the production of meaningful results. In particular, the values of $K_D$ obtained from the intercept of the above-mentioned straight line (see Equation 14) were unreliable in all cases. In this respect, Figure 36 shows, as an example, the plot obtained for $L\alpha_H$.

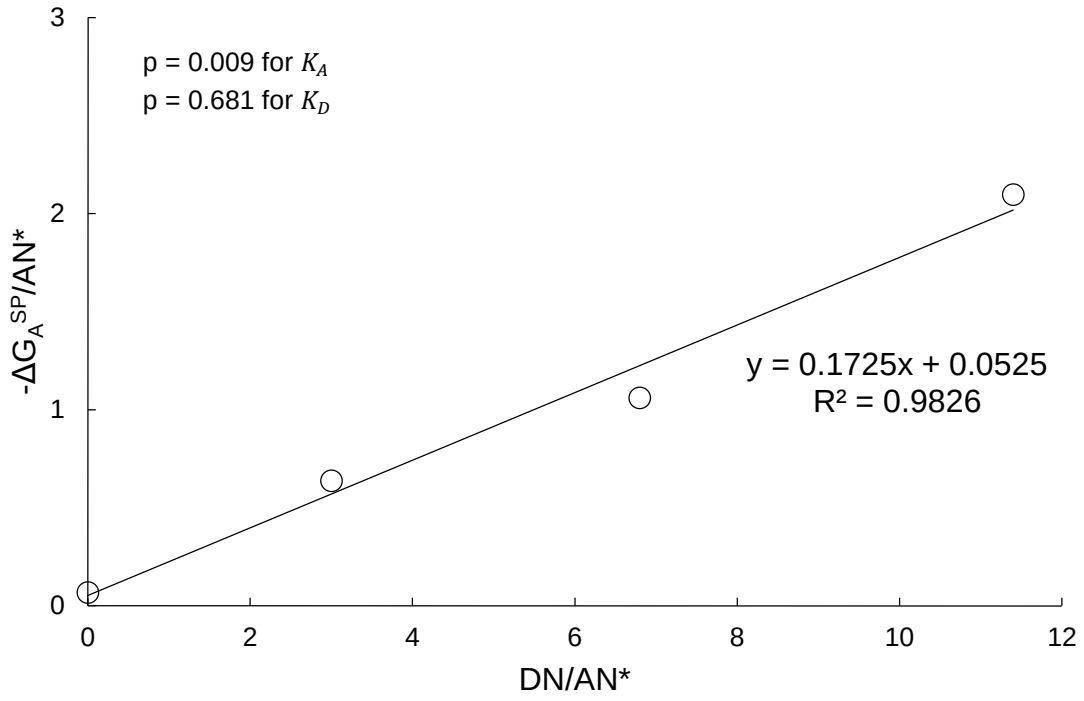


**Figure 36** $-\Delta G_A^{SP}/AN^*$ *vs* $DN/AN^*$ plot obtained for $L\alpha_H$.

While the slope of the line obtained from the linear regression of the experimental data ($K_A$ parameter) was statistically significant (p = 0.009), the intercept ($K_D$ parameter) was statistically not different from zero (p = 0.681).

Differently, the van Oss approach was successfully applied. From the injection of ethyl acetate (employed as monopolar basic probe) and chloroform (used as monopolar acidic probe), the acid ($\gamma_S^+$) and the base ($\gamma_S^-$) contributions of specific surface energy were determined for all the samples under investigation (Figure 37).

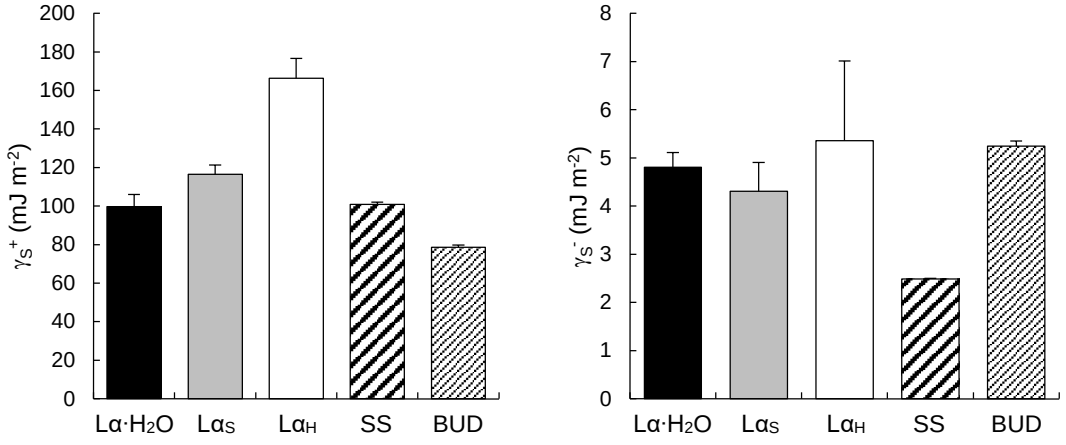


**Figure 37** Acid ($\gamma_S^+$, left panel) and base ($\gamma_S^-$, right panel) contributions of the specific surface energy of lactose carriers and APIs.

These results showed particularly interesting trends. Lactose carriers gave progressively stronger interactions with the electron donating ethyl acetate, following the order $L\alpha{\cdot}H_2O < L\alpha_S < L\alpha_H$. This was indicative of the more acidic character of $L\alpha_S$, and especially $L\alpha_H$, with respect to $L\alpha{\cdot}H_2O$. A possible explanation could be the increased propensity of $L\alpha_H$ to form hydrogen bonds as a result of the removal of crystalline water. Differently, reactivity towards the acidic chloroform did not show a statistically significant difference (ANOVA, p > 0.05). As far as the APIs are concerned, salbutamol sulphate exhibited higher acidic character (as proved by the stronger interaction with ethyl acetate) than

budesonide. This was consistent with the interactions of the two APIs towards chloroform, showing budesonide higher propensity to electron donation.

The highlighted tendencies may be exploited to explain, at least in part, the opposite trend observed in the aerosolization performance of the mixtures containing salbutamol sulphate and budesonide. The combination of salbutamol sulphate with a carrier having an increased acidic character ($L\alpha_H > L\alpha_S > L\alpha \cdot H_2O$) might have led to unfavorable drug-carrier interactions, thus resulting in a higher FPF. An opposite tendency would be expected for budesonide.

### 4.4.4. Total Surface Energy

$\gamma_S^+$ and $\gamma_S^-$ were used to calculate the specific surface energy, $\gamma_S^{SP}$, according to Equation 16. $\gamma_S^{SP}$ was then added to $\gamma_S^D$ to obtain the total surface energy $\gamma_S$ (Table 11).

**Table 11** Dispersive ($\gamma_S^D$), specific ($\gamma_S^{SP}$) and total surface energy ($\gamma_S$) of lactose carriers and APIs.

| Sample | $\gamma_S^D$ (mJ m$^{-2}$) | $\gamma_S^{SP}$ (mJ m$^{-2}$) | $\gamma_S$ (mJ m$^{-2}$) |
|---|---|---|---|
| $L\alpha \cdot H_2O$ | 27.8 | 43.8 | 71.5 |
| $L\alpha_S$ | 35.4 | 44.7 | 80.1 |
| $L\alpha_H$ | 36.3 | 59.2 | 95.5 |
| SS | 45.5 | 31.6 | 77.2 |
| BUD | 44.5 | 40.6 | 85.1 |

Among lactose carriers, $L\alpha_H$ showed the highest total surface energy. This is consistent with the fact that it is more thermodynamically unstable with respect to the other two polymorphs. Quite surprisingly budesonide showed a specific surface energy higher than that of salbutamol sulphate. This may appear in contradiction with the characteristics of

the two drugs in terms of hydrophilicity. However, it should be taken into account that, in this case, analyses were performed on samples in the solid state, while the acid-base properties considered in the common knowledge refer to molecules/ions in solution, namely in conditions where the interactions among the same species are minimal or absent.

The relationship between the total surface energy of lactose carriers and the FPFs obtained with the tested mixtures was evaluated according to the approach reported by Traini et al. (Traini et al., 2008) (Figure 38).

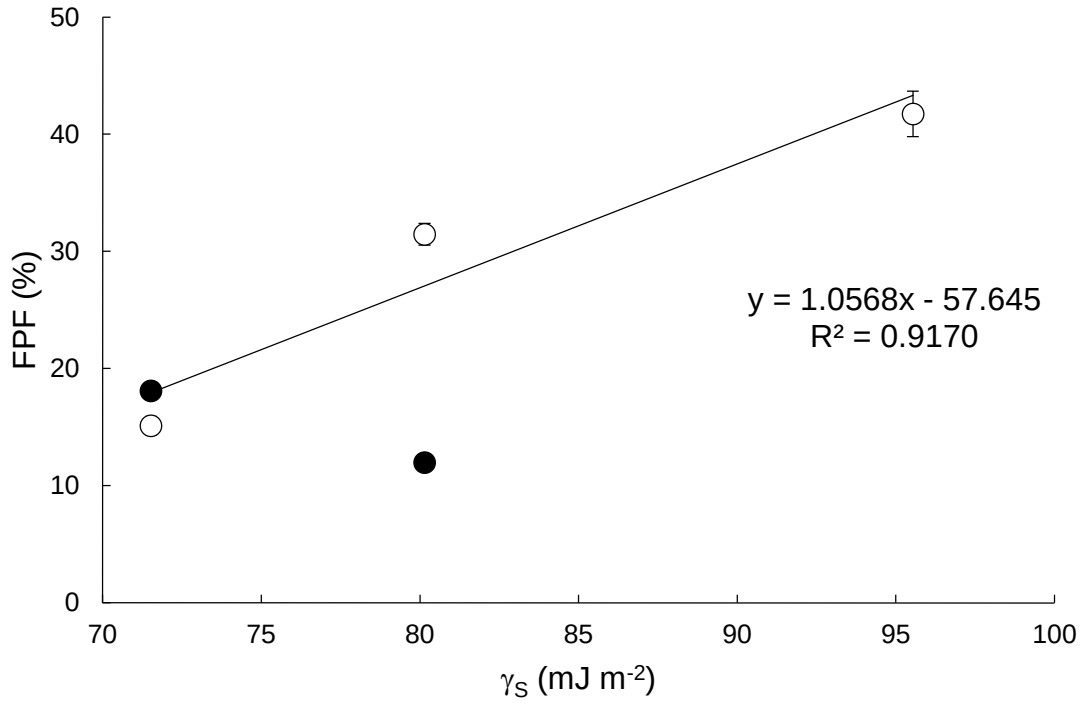


**Figure 38** Fine particle fraction (FPF) *vs* total surface energy ($\gamma_S$) of lactose carriers for the tested mixtures containing salbutamol sulphate (empty circle) and budesonide (solid circle). Linear regression refers only to salbutamol sulphate data.

In their work, Traini et al. found an inverse linear relationship between carrier surface energy and salbutamol sulphate aerosolization efficiency. Such results were in agreement

with the common idea that an increased surface energy implies a stronger adhesion between carrier and drug particles, leading to decreased aerosolization performance.

Opposite results were, instead, reported by Cline and Dalby (Cline and Dalby, 2002), who described improved FPFs of different drugs with increasing carrier-drug interactions. This counterintuitive finding was justified claiming that a certain minimum interaction between carrier and drug particles is needed in order to break drug agglomerates and promote aerosolization upon inhalation. However, the approach of these authors was later criticized by Chow et al. (Chow et al., 2004) on both technical and fundamental aspects.

As regards the results hereby presented, while in the case of budesonide a trend similar to that reported by Traini et al. would be plausible, in the case of salbutamol sulphate the existence of an opposite correlation seemed more likely. In fact, the use of carriers with increased surface energy produced higher FPFs (Figure 38).

Similar results were reported also by Bernhard and Steckel (Bernhard and Steckel, 2005), who combined the surface energy of different lactose carriers with their specific surface area and found a positive correlation with the fine particle delivery of salbutamol sulphate and a negative correlation for budesonide.

In such a contest, it becomes clear that the prediction of DPI performance from the measurement of a single parameter, such as the carrier surface energy, is unlikely to be successful. Many different variables other than surface energy (such as the different carrier roughness and fine particle content in this specific case) may affect the interaction between carrier and drug particles. Moreover, the evaluation of the overall balance between drug-carrier adhesion and the dispersion forces generated within the inhaler device upon inhalation, rather than an increased or decreased carrier surface energy, would be more useful to determine the efficiency of the aerosolization performance.

# *Conclusions*

# 5. CONCLUSIONS

The present research project has been focused on the study of the effect of lactose solid-state on the aerosolization performance of drug-carrier mixtures for inhalation.

Particular attention was devoted to the evaluation of the impact of the micronization process on the physico-chemical properties of lactose.

$^1$H NMR was employed to characterize micronized lactose samples in terms of anomeric composition, demonstrating that the micronization of L$\alpha\cdot H_2O$ in the used conditions does not result in the formation of β-lactose. Further characterization by XRPD and DSC pointed out that micronized lactose assumes solid-state characteristics different from those of the starting material. In particular, DSC was successfully used to identify the different solid phases of lactose induced by the process. L$\alpha_H$ and amorphous α-lactose may both be produced in variable amounts depending on the energetics of the micronization. In particular, the formation of L$\alpha_H$ represents a new finding, as literature generally reports only the formation of amorphous material as a consequence of the mechanical stress stemming from the micronization. However, due to the partial overlapping of the characteristic thermal events, DSC is not suitable for the quantification of L$\alpha_H$ and amorphous lactose when they are simultaneously present in the same sample. For this reason, a new gravimetric method based on DVS measurements was developed for the identification and quantification of different forms of lactose (L$\alpha_H$, L$\alpha_S$ and amorphous α-lactose). The method is very simple and provides acceptable accuracy in phase quantitation. Its application to a sample of micronized lactose produced on an industrial scale led to results in agreement with those obtained by DSC and evidenced that L$\alpha_H$, rather than amorphous lactose, is generated in the micronization process. The

major limitation of the developed method is that it can be used to analyse only samples consisting of 100% α-lactose (or containing negligible percentages of β-form). On the other hand, this approach may find a more general application for the quantification of polymorphs of compounds different than lactose, provided that the various solid phases afford different weight variations in specific regions of the DVS profile.

One of the samples of micronized lactose was then selected to be used as fine component in the preparation of ternary mixtures containing $L\alpha \cdot H_2O$ as carrier and salbutamol sulphate as model API. The presence of a fixed amount of fine lactose (i.e., 30% w/w) in the mixture resulted in a remarkable positive effect on the aerosolization performance. However, this positive effect decreased and eventually disappeared with the aging of the mixtures. A concomitant change in the solid-state of fine micronized lactose was observed by DSC. Thus, it was speculated that the positive effect of lactose fines depends, not only on their reduced size, but also on a specific characteristic of their solid-state leading to the decrease of the surface interaction with the drug and consequent improvement of the respirability of the latter. This hypothesis is supported by specific aerosolization experiments carried out with binary mixtures employing, as carriers, different polymorphs of lactose. The use of practically fine-free $L\alpha_S$, and especially $L\alpha_H$ (in place of the traditional $L\alpha \cdot H_2O$), led to significantly improved respirability of salbutamol sulphate, thus confirming the key role of lactose solid-state in affecting the aerosolization performance. Differently, the use of $L\alpha_S$ in place of $L\alpha \cdot H_2O$ in binary mixtures with budesonide led to poorer performance. On the basis of the obtained results, it was speculated that hydrophilic drugs (such as salbutamol sulphate) would benefit from the use, as carrier, of an anhydrous form of lactose, while more lipophilic drugs (such as budesonide) would rather require the use of conventional α-lactose monohydrate.

In the light of these considerations, IGC was selected as a tool to investigate possible variations in the surface energy of the lactose carriers and the APIs under investigation. A direct correlation between the total surface energy of lactose carriers and the FPFs obtained for the two drugs was not found. The difference in the specific (acid-base) interactions exhibited by the drugs may account for the opposite tendency of the aerosolization performance when they were combined with carriers showing different electron accepting propensity.

As a general conclusion, it is unrealistic to expect that a single parameter, such as surface energy, could be used to predict the performance of aerosolization. Many different factors other than surface energy, such as those described in the present study, may participate in determining the interactions between carrier and drug particles. Moreover, the overall balance between drug-carrier adhesion and the dispersion forces generated by the inhaler device should not be disregarded.

# *References*

# 6. REFERENCES

Atkins, P.J., 2005. Dry Powder Inhalers: An Overview. Respiratory Care 50, 1304-1312.

Aulton, M.E., Taylor, K.M.G., 2013. Aulton's Pharmaceutics: The Design and Manufacture of Medicines. Churchill Livingstone Elsevier.

Beevers, C.A., Hansen, H.N., 1971. The Structure of α-Lactose Monohydrate. Acta Crystallographica Section B 27, 1323-1325.

Begat, P., Morton, D.V., Staniforth, J., Price, R., 2004a. The Cohesive-Adhesive Balances in Dry Powder Inhaler Formulations I: Direct Quantification by Atomic Force Microscopy. Pharm Res 21, 1591-1597.

Begat, P., Morton, D.V., Staniforth, J., Price, R., 2004b. The Cohesive-Adhesive Balances in Dry Powder Inhaler Formulations II: Influence on Fine Particle Delivery Characteristics. Pharm Res 21, 1826-1833.

Benet, L.Z., Broccatelli, F., Oprea, T.I., 2011. BDDCS Applied to Over 900 Drugs. The AAPS journal 13, 519-547.

Berkenfeld, K., Lamprecht, A., McConville, J., 2015. Devices for Dry Powder Drug Delivery to the Lung. AAPS PharmSciTech 16, 479-490.

Bernhard, F., Steckel, H., 2005. Proposing a Model That Correlates Surface Energy Values to Aerosol Data, Proceedings of Drug Delivery to the Lungs 16.

Briggner, L.-E., Buckton, G., Bystrom, K., Darcy, P., 1994. The Use of Isothermal Microcalorimetry in the Study of Changes in Crystallinity Induced During the Processing of Powders. International Journal of Pharmaceutics 105, 125-135.

Buckton, G., 1997. Characterisation of Small Changes in the Physical Properties of Powders of Significance for Dry Powder Inhaler Formulations. Advanced Drug Delivery Reviews 26, 17-27.

Buckton, G., Darcy, P., 1995. The Use of Gravimetric Studies to Assess the Degree of Crystallinity of Predominantly Crystalline Powders. International Journal of Pharmaceutics 123, 265-271.

Buckton, G., Darcy, P., 1999. Assessment of Disorder in Crystalline Powders — A Review of Analytical Techniques and Their Application. International Journal of Pharmaceutics 179, 141-158.

Buckton, G., Gill, H., 2007. The Importance of Surface Energetics of Powders for Drug Delivery and the Establishment of Inverse Gas Chromatography. Advanced Drug Delivery Reviews 59, 1474-1479.

Burnett, D., Malde, N., Williams, D., 2009. Characterizing Amorphous Materials with Gravimetric Vapour Sorption Techniques. Pharmaceutical Technology Europe 21.

Carstensen, J.T., 2001. Advanced Pharmaceutical Solids.

Chow, A.H., Tong, H.H., Chattopadhyay, P., Shekunov, B.Y., 2007. Particle Engineering for Pulmonary Drug Delivery. Pharm Res 24, 411-437.

Chow, A.H., Tong, H.H., Shekunov, B.Y., York, P., 2004. Use of Inverse Gas Chromatography (IGC) to Determine the Surface Energy and Surface Area of Powdered Materials. Pharm Res 21, 1718-1719; author reply 1719-1720.

Claus, S., Weiler, C., Schiewe, J., Friess, W., 2014. How Can We Bring High Drug Doses to the Lung? European Journal of Pharmaceutics and Biopharmaceutics 86, 1-6.

Cline, D., Dalby, R., 2002. Predicting the Quality of Powders for Inhalation from Surface Energy and Area. Pharm Res 19, 1274-1277.

Colombo, P., Traini, D., Buttini, F., 2013. Inhalation Drug Delivery: Techniques and Products. John Wiley & Sons, Ltd.

Craig, D.Q.M., Reading, M., 2007. Thermal Analysis of Pharmaceuticals.

de Boer, A.H., Chan, H.K., Price, R., 2012. A Critical View on Lactose-Based Drug Formulation and Device Studies for Dry Powder Inhalation: Which Are Relevant and What Interactions to Expect? Advanced Drug Delivery Reviews 64, 257-274.

Dickhoff, B.H.J., de Boer, A.H., Lambregts, D., Frijlink, H.W., 2006. The Effect of Carrier Surface Treatment on Drug Particle Detachment from Crystalline Carriers in Adhesive Mixtures for Inhalation. International Journal of Pharmaceutics 327, 17-25.

Donovan, M.J., Smyth, H.D.C., 2010. Influence of Size and Surface Roughness of Large Lactose Carrier Particles in Dry Powder Inhaler Formulations. International Journal of Pharmaceutics 402, 1-9.

Earl, W.L., Parrish, F.W., 1983. A Cross-Polarization-Magic-Angle Sample Spinning N.M.R. Study of Several Crystal Forms of Lactose. Carbohydrate Research 115, 23-32.

Edwards, D.A., Hanes, J., Caponetti, G., Hrkach, J., Ben-Jebria, A., Eskew, M.L., Mintzes, J., Deaver, D., Lotan, N., Langer, R., 1997. Large Porous Particles for Pulmonary Drug Delivery. Science (New York, N.Y.) 276, 1868-1871.

Ferrari, F., Cocconi, D., Bettini, R., Giordano, F., Santi, P., Tobyn, M., Price, R., Young, P., Caramella, C., Colombo, P., 2004. The Surface Roughness of Lactose Particles Can Be Modulated by Wet-Smoothing Using a High-Shear Mixer. AAPS PharmSciTech 5, 69-74.

Figura, L., Epple, M., 1995. Anhydrous α-Lactose. A Study with DSC and TXRD. Journal of Thermal Analysis and Calorimetry 44, 45-53.

Fries, D.C., Rao, S.T., Sundaralingam, M., 1971. Structural Chemistry of Carbohydrates. III. Crystal and Molecular Structure of 4-*O*-β-D-Galactopyranosyl-α-D-Glucopyranose Monohydrate (α-Lactose Monohydrate). Acta Crystallographica Section B 27, 994-1005.

Frijlink, H.W., De Boer, A.H., 2004. Dry Powder Inhalers for Pulmonary Drug Delivery. Expert opinion on drug delivery 1, 67-86.

Garnier, S., Petit, S., Coquerel, G., 2002. Dehydration Mechanism and Crystallisation Behaviour of Lactose. Journal of Thermal Analysis and Calorimetry 68, 489-502.

Garnier, S., Petit, S., Mallet, F., Petit, M.N., Lemarchand, D., Coste, S., Lefebvre, J., Coquerel, G., 2008. Influence of Ageing, Grinding and Preheating on the Thermal Behaviour of α-Lactose Monohydrate. International Journal of Pharmaceutics 361, 131-140.

Geller, D.E., Weers, J., Heuerding, S., 2011. Development of an Inhaled Dry-Powder Formulation of Tobramycin Using PulmoSphere™ Technology. Journal of Aerosol Medicine and Pulmonary Drug Delivery 24, 175-182.

Gombás, Á., Szabó-Révész, P., Kata, M., Regdon, G., Jr., Erős, I., 2002. Quantitative Determination of Crystallinity of α-Lactose Monohydrate by DSC. Journal of Thermal Analysis and Calorimetry 68, 503-510.

Grasmeijer, F., Lexmond, A.J., van den Noort, M., Hagedoorn, P., Hickey, A.J., Frijlink, H.W., de Boer, A.H., 2014. New Mechanisms to Explain the Effects of Added Lactose Fines on the Dispersion Performance of Adhesive Mixtures for Inhalation. PloS one 9, e87825.

Grimsey, I.M., Feeley, J.C., York, P., 2002. Analysis of the Surface Energy of Pharmaceutical Powders by Inverse Gas Chromatography. Journal of Pharmaceutical Sciences 91, 571-583.

Guenette, E., Barrett, A., Kraus, D., Brody, R., Harding, L., Magee, G., 2009. Understanding the Effect of Lactose Particle Size on the Properties of DPI Formulations Using Experimental Design. International Journal of Pharmaceutics 380, 80-88.

Gutmann, V., 1978. The Donor-Acceptor Approach to Molecular Interactions.

Heng, P.W.S., Chan, L.W., Lim, L.T., 2000. Quantification of the Surface Morphologies of Lactose Carriers and Their Effect on the *in Vitro* Deposition of Salbutamol Sulphate. Chemical and Pharmaceutical Bulletin 48, 393-398.

Hickey, A.J., Mansour, H.M., Telko, M.J., Xu, Z., Smyth, H.D., Mulder, T., McLean, R., Langridge, J., Papadopoulos, D., 2007. Physical Characterization of Component Particles Included in Dry Powder Inhalers. I. Strategy Review and Static Characteristics. Journal of Pharmaceutical Sciences 96, 1282-1301.

Hill, V.L., Craig, D.Q.M., Feely, L.C., 1998. Characterisation of Spray-Dried Lactose Using Modulated Differential Scanning Calorimetry. International Journal of Pharmaceutics 161, 95-107.

Hirotsu, K., Shimada, A., 1974. The Crystal and Molecular Structure of β-Lactose. Bulletin of the Chemical Society of Japan 47, 1872-1879.

Hoppentocht, M., Hagedoorn, P., Frijlink, H.W., de Boer, A.H., 2014. Technological and Practical Challenges of Dry Powder Inhalers and Formulations. Advanced Drug Delivery Reviews 75, 18-31.

Iida, K., Hayakawa, Y., Okamoto, H., Danjo, K., Leuenberger, H., 2003. Preparation of Dry Powder Inhalation by Surface Treatment of Lactose Carrier Particles. Chemical and Pharmaceutical Bulletin 51, 1-5.

Jawad, R., Elleman, C., Vermeer, L., Drake, A., Woodhead, B., Martin, G., Royall, P., 2012. The Measurement of the β/α Anomer Composition Within Amorphous Lactose Prepared by Spray and Freeze Drying Using a Simple $^{1}$H-NMR Method. Pharm Res 29, 511-524.

Jones, M.D., Harris, H., Hooton, J.C., Shur, J., King, G.S., Mathoulin, C.A., Nichol, K., Smith, T.L., Dawson, M.L., Ferrie, A.R., Price, R., 2008a. An Investigation into the Relationship Between Carrier-Based Dry Powder Inhalation Performance and Formulation Cohesive–Adhesive Force Balances. European Journal of Pharmaceutics and Biopharmaceutics 69, 496-507.

Jones, M.D., Hooton, J.C., Dawson, M.L., Ferrie, A.R., Price, R., 2008b. An Investigation into the Dispersion Mechanisms of Ternary Dry Powder Inhaler Formulations by the Quantification of Interparticulate Forces. Pharm Res 25, 337-348.

Jones, M.D., Price, R., 2006. The Influence of Fine Excipient Particles on the Performance of Carrier-Based Dry Powder Inhalation Formulations. Pharm Res 23, 1665-1674.

Jones, M.D., Santo, J.G.F., Yakub, B., Dennison, M., Master, H., Buckton, G., 2010. The Relationship Between Drug Concentration, Mixing Time, Blending Order and Ternary Dry Powder Inhalation Performance. International Journal of Pharmaceutics 391, 137-147.

Jones, M.D., Young, P., Traini, D., 2012. The Use of Inverse Gas Chromatography for the Study of Lactose and Pharmaceutical Materials Used in Dry Powder Inhalers. Advanced Drug Delivery Reviews 64, 285-293.

Kaialy, W., Alhalaweh, A., Velaga, S.P., Nokhodchi, A., 2012a. Influence of Lactose Carrier Particle Size on the Aerosol Performance of Budesonide from a Dry Powder Inhaler. Powder Technology 227, 74-85.

Kaialy, W., Ticehurst, M., Nokhodchi, A., 2012b. Dry Powder Inhalers: Mechanistic Evaluation of Lactose Formulations Containing Salbutamol Sulphate. International Journal of Pharmaceutics 423, 184-194.

Kawashima, Y., Serigano, T., Hino, T., Yamamoto, H., Takeuchi, H., 1998. Effect of Surface Morphology of Carrier Lactose on Dry Powder Inhalation Property of Pranlukast Hydrate. International Journal of Pharmaceutics 172, 179-188.

Kinnunen, H., Hebbink, G., Peters, H., Huck, D., Makein, L., Price, R., 2015. Extrinsic Lactose Fines Improve Dry Powder Inhaler Formulation Performance of a Cohesive Batch of Budesonide via Agglomerate Formation and Consequential Co-Deposition. International Journal of Pharmaceutics 478, 53-59.

Kirch, J., Schneider, A., Abou, B., Hopf, A., Schaefer, U.F., Schneider, M., Schall, C., Wagner, C., Lehr, C.-M., 2012. Optical Tweezers Reveal Relationship Between Microstructure and Nanoparticle Penetration of Pulmonary Mucus. Proceedings of the National Academy of Sciences 109, 18355-18360.

Kirk, J.H., Dann, S.E., Blatchford, C.G., 2007. Lactose: A Definitive Guide to Polymorph Determination. International Journal of Pharmaceutics 334, 103-114.

Kou, X., Chan, L.W., Steckel, H., Heng, P.W.S., 2012. Physico-Chemical Aspects of Lactose for Inhalation. Advanced Drug Delivery Reviews 64, 220-232.

Larhrib, H., Martin, G.P., Marriott, C., Prime, D., 2003a. The Influence of Carrier and Drug Morphology on Drug Delivery from Dry Powder Formulations. International Journal of Pharmaceutics 257, 283-296.

Larhrib, H., Martin, G.P., Prime, D., Marriott, C., 2003b. Characterisation and Deposition Studies of Engineered Lactose Crystals with Potential for Use as a Carrier for Aerosolised Salbutamol Sulfate from Dry Powder Inhalers. European Journal of Pharmaceutical Sciences 19, 211-221.

Larhrib, H., Zeng, X.M., Martin, G.P., Marriott, C., Pritchard, J., 1999. The Use of Different Grades of Lactose as a Carrier for Aerosolised Salbutamol Sulphate. International Journal of Pharmaceutics 191, 1-14.

Lefebvre, J., Willart, J.-F., Caron, V., Lefort, R., Affouard, F., Danede, F., 2005. Structure Determination of the 1/1 α/β Mixed Lactose by X-Ray Powder Diffraction. Acta Crystallographica Section B 61, 455-463.

Lerk, C.F., Andreae, A.C., de Boer, A.H., de Hoog, P., Kussendrager, K., van Leverink, J., 1984a. Alterations of α-Lactose During Differential Scanning Calorimetry. Journal of Pharmaceutical Sciences 73, 856-857.

Lerk, C.F., Andreae, A.C., de Boer, A.H., de Hoog, P., Kussendrager, K., van Leverink, J., 1984b. Transitions of Lactoses by Mechanical and Thermal Treatment. Journal of Pharmaceutical Sciences 73, 857-859.

Louey, M.D., Razia, S., Stewart, P.J., 2003. Influence of Physico-Chemical Carrier Properties on the in Vitro Aerosol Deposition from Interactive Mixtures. International Journal of Pharmaceutics 252, 87-98.

Louey, M.D., Stewart, P.J., 2002. Particle Interactions Involved in Aerosol Dispersion of Ternary Interactive Mixtures. Pharm Res 19, 1524-1531.

Lucas, P., Anderson, K., Staniforth, J.N., 1998. Protein Deposition from Dry Powder Inhalers: Fine Particle Multiplets as Performance Modifiers. Pharm Res 15, 562-569.

Marriott, C., Frijlink, H.W., 2012. Lactose as a Carrier for Inhalation Products: Breathing New Life into an Old Carrier. Advanced Drug Delivery Reviews 64, 217-219.

Otsuka, M., Ohtani, H., Kaneniwa, N., Higuchi, S., 1991. Isomerization of Lactose in Solid-State by Mechanical Stress During Grinding. Journal of Pharmacy and Pharmacology 43, 148-153.

Patton, J.S., Byron, P.R., 2007. Inhaling Medicines: Delivering Drugs to the Body Through the Lungs. Nature Reviews Drug Discovery 6, 67-74.

Pilcer, G., Wauthoz, N., Amighi, K., 2012. Lactose Characteristics and the Generation of the Aerosol. Advanced Drug Delivery Reviews 64, 233-256.

Pitchayajittipong, C., Price, R., Shur, J., Kaerger, J.S., Edge, S., 2010. Characterisation and Functionality of Inhalation Anhydrous Lactose. International Journal of Pharmaceutics 390, 134-141.

Platteau, C., Lefebvre, J., Affouard, F., Derollez, P., 2004. *Ab Initio* Structure Determination of the Hygroscopic Anhydrous Form of α-Lactose by Powder X-Ray Diffraction. Acta Crystallographica Section B 60, 453-460.

Platteau, C., Lefebvre, J., Affouard, F., Willart, J.-F., Derollez, P., Mallet, F., 2005. Structure Determination of the Stable Anhydrous Phase of α-Lactose from X-Ray Powder Diffraction. Acta Crystallographica Section B 61, 185-191.

Riddle, F.L., Fowkes, F.M., 1990. Spectral Shifts in Acid-Base Chemistry. 1. Van der Waals Contributions to Acceptor Numbers. Journal of the American Chemical Society 112, 3259-3264.

Saleki-Gerhardt, A., Ahlneck, C., Zografi, G., 1994. Assessment of Disorder in Crystalline Solids. International Journal of Pharmaceutics 101, 237-247.

Schultz, J., Lavielle, L., Martin, C., 1987. The Role of the Interface in Carbon Fibre-Epoxy Composites. The Journal of Adhesion 23, 45-60.

Shah, B., Kakumanu, V.K., Bansal, A.K., 2006. Analytical Techniques for Quantification of Amorphous/Crystalline Phases in Pharmaceutical Solids. Journal of Pharmaceutical Sciences 95, 1641-1665.

Shariare, M.H., de Matas, M., York, P., Shao, Q., 2011. The Impact of Material Attributes and Process Parameters on the Micronisation of Lactose Monohydrate. International Journal of Pharmaceutics 408, 58-66.

Sheokand, S., Modi, S.R., Bansal, A.K., 2014. Dynamic Vapor Sorption as a Tool for Characterization and Quantification of Amorphous Content in Predominantly Crystalline Materials. Journal of Pharmaceutical Sciences 103, 3364-3376.

Shur, J., Harris, H., Jones, M.D., Kaerger, J.S., Price, R., 2008. The Role of Fines in the Modification of the Fluidization and Dispersion Mechanism Within Dry Powder Inhaler Formulations. Pharm Res 25, 1631-1640.

Smith, I.J., Parry-Billings, M., 2003. The Inhalers of the Future? A Review of Dry Powder Devices on the Market Today. Pulmonary Pharmacology & Therapeutics 16, 79-95.

Smith, J.H., Dann, S.E., Elsegood, M.R.J., Dale, S.H., Blatchford, C.G., 2005. α-Lactose Monohydrate: A Redetermination at 150 K. Acta Crystallographica Section E 61, o2499-o2501.

Sonneveld, E.J., Visser, J.W., 1975. Automatic Collection of Powder Data from Photographs. Journal of Applied Crystallography 8, 1-7.

Steckel, H., Markefka, P., teWierik, H., Kammelar, R., 2006. Effect of Milling and Sieving on Functionality of Dry Powder Inhalation Products. International Journal of Pharmaceutics 309, 51-59.

Telko, M.J., Hickey, A.J., 2005. Dry Powder Inhaler Formulation. Respiratory Care 50, 1209-1227.

Timmermann, I.-L., Steckel, H., Trunk, M., 2006. Assessing the Re-Crystallization Behaviour of Amorphous Lactose Using the RH-Perfusion Cell. European Journal of Pharmaceutics and Biopharmaceutics 64, 107-114.

Timsina, M.P., Martin, G.P., Marriott, C., Ganderton, D., Yianneskis, M., 1994. Drug Delivery to the Respiratory Tract Using Dry Powder Inhalers. International Journal of Pharmaceutics 101, 1-13.

Tong, H.H.Y., Shekunov, B.Y., York, P., Chow, A.H.L., 2002. Influence of Polymorphism on the Surface Energetics of Salmeterol Xinafoate Crystallized from Supercritical Fluids. Pharm Res 19, 640-648.

Traini, D., Young, P.M., Thielmann, F., Acharya, M., 2008. The Influence of Lactose Pseudopolymorphic Form on Salbutamol Sulfate-Lactose Interactions in DPI Formulations. Drug development and industrial pharmacy 34, 992-1001.

van Oss, C.J., 2006. Interfacial Forces in Aqueous Media. CRC Press.

Vollenbroek, J., Hebbink, G.A., Ziffels, S., Steckel, H., 2010. Determination of Low Levels of Amorphous Content in Inhalation Grade Lactose by Moisture Sorption Isotherms. International Journal of Pharmaceutics 395, 62-70.

Voss, A., Finlay, W.H., 2002. Deagglomeration of Dry Powder Pharmaceutical Aerosols. International Journal of Pharmaceutics 248, 39-50.

Weibel, E.R., 1963. Morphometry of the Human Lung.

Willart, J.F., Caron, V., Lefort, R., Danède, F., Prévost, D., Descamps, M., 2004. Athermal Character of the Solid State Amorphization of Lactose Induced by Ball Milling. Solid State Communications 132, 693-696.

Young, P.M., Chan, H.-K., Chiou, H., Edge, S., Tee, T.H.S., Traini, D., 2007. The Influence of Mechanical Processing of Dry Powder Inhaler Carriers on Drug Aerosolization Performance. Journal of Pharmaceutical Sciences 96, 1331-1341.

Young, P.M., Cocconi, D., Colombo, P., Bettini, R., Price, R., Steele, D.F., Tobyn, M.J., 2002. Characterization of a Surface Modified Dry Powder Inhalation Carrier Prepared by "Particle Smoothing". Journal of Pharmacy and Pharmacology 54, 1339-1344.

Zeng, X.-M., Martin, G.P., Marriott, C., Pritchard, J., 2001a. Lactose as a Carrier in Dry Powder Formulations: The Influence of Surface Characteristics on Drug Delivery. Journal of Pharmaceutical Sciences 90, 1424-1434.

Zeng, X.M., Martin, G.P., Marriott, C., Pritchard, J., 2000a. The Effects of Carrier Size and Morphology on the Dispersion of Salbutamol Sulphate after Aerosolization at Different Flow Rates. Journal of Pharmacy and Pharmacology 52, 1211-1221.

Zeng, X.M., Martin, G.P., Marriott, C., Pritchard, J., 2000b. The Influence of Carrier Morphology on Drug Delivery by Dry Powder Inhalers. International Journal of Pharmaceutics 200, 93-106.

Zeng, X.M., Martin, G.P., Marriott, C., Pritchard, J., 2000c. The Influence of Crystallization Conditions on the Morphology of Lactose Intended for Use as a Carrier for Dry Powder Aerosols. Journal of Pharmacy and Pharmacology 52, 633-643.

Zeng, X.M., Martin, G.P., Marriott, C., Pritchard, J., 2001b. The Use of Lactose Recrystallised from Carbopol Gels as a Carrier for Aerosolised Salbutamol Sulphate. European Journal of Pharmaceutics and Biopharmaceutics 51, 55-62.

Zeng, X.M., Martin, G.P., Tee, S.-K., Ghoush, A.A., Marriott, C., 1999. Effects of Particle Size and Adding Sequence of Fine Lactose on the Deposition of Salbutamol Sulphate from a Dry Powder Formulation. International Journal of Pharmaceutics 182, 133-144.

Zeng, X.M., Martin, G.P., Tee, S.-K., Marriott, C., 1998. The Role of Fine Particle Lactose on the Dispersion and Deaggregation of Salbutamol Sulphate in an Air Stream in Vitro. International Journal of Pharmaceutics 176, 99-110.

Zeng, X.M., Pandhal, K.H., Martin, G.P., 2000d. The Influence of Lactose Carrier on the Content Homogeneity and Dispersibility of Beclomethasone Dipropionate from Dry Powder Aerosols. International Journal of Pharmaceutics 197, 41-52.

## Acknowledgments

The present research project was developed in collaboration with Micro-Sphere SA, that is kindly acknowledged for providing most of the studied materials and for the financial support.

I am very grateful to Prof. Ruggero Bettini for his support and assistance throughout the years I spent at the University of Parma.

Finally, I would like to thank Prof. Teresa Carvajal and Prof. Rodolfo Pinal for giving me the opportunity to carry out part of the work at the Purdue University in West Lafayette.